Research report (homologation with the double degree program ENSIC-UIS):

Synthesis and development of high-performance composite polymer membranes for CO2 capture.

By:

María Valentina Velasco Rueda

A thesis submitted in partial fulfillment of the requirements for the degree of Master of Chemical Engineering

Directed by:

Dr. Anne Jonquières

Dr. Carlos Jesus Muvdi Nova

Universidad Industrial de Santander

Facultad de Ingenierías Fisicoquímicas

Escuela de Ingeniería Química

Maestría en Ingeniería Química

2025

Acknowledgments

This project could not have been possible without the wonderful guidance and patience of my four supervisors: Anne Jonquières, Carole Arnal-Herault, Carlos Jesus Muvdi Nova, and Bouchra Belaissaoui. Their investment and love for the project inspired me and I'm really thankful for the last 5 months that I have been able to share with them.

I would like to also thank Thomas Arzoumanian for providing a series of characterizations of the elaborated material and giving the first steps so that I could follow with the project. Thanks to Jean Claude Sivault for the amazing work conceiving the time-lag and always answering our questions and requests. Also, thanks to Olivier Fabre for the NMR analysis.

I would also like to thank Anamaria Barrera, who always ready to help and listen to me whenever I needed her. I'm deeply grateful to my mom, my sister, and my dad. I would not be who I am and achieved what I have done without them.

Table of contents

List of Figures

List of tables

Resumen

Título: Síntesis y desarollo de membranas poliméricas composites de alto rendimiento para la captura de CO_2*

Autor: Maria Valentina Velasco Rueda**

Palabras clave: Polímero, membranas a matriz mixta, membranas para la captura de CO_2, PUI, redes metal organicas

Descripción: Para abordar los desafíos asociados al cambio climático y al calentamiento global, los procesos de separación mediante membranas se consideran soluciones industriales innovadoras. Entre los diferentes materiales poliméricos empleados en membranas, las membranas de matriz mixta (MMM, por sus siglas en inglés) resultan altamente prometedoras para la captura de CO_2. En este trabajo, se seleccionó como nueva matriz polimérica elastomérica un poli(urea-imida) segmentado con un alto contenido de poli(óxido de etileno) (70 % en peso), el cual fue dopado con la estructura metal-orgánica ZIF-8.

La introducción de esta nueva matriz polimérica, junto con la optimización del método de "preacondicionamiento" (priming), permitió alcanzar cargas de ZIF-8 excepcionalmente elevadas, hasta un 70 % en volumen. Se emplearon diversos métodos fisicoquímicos para estudiar la influencia de las interacciones entre el relleno y el polímero sobre la morfología de la membrana.

Las propiedades de permeación de CO_2 y N_2 se evaluaron mediante mediciones de time-lag para gases puros, bajo condiciones estándar de captura postcombustión de CO_2 (2 bar y 35 °C). Se obtuvieron resultados muy prometedores para la carga más alta de ZIF-8 (70 % vol), con un incremento significativo en la permeabilidad al CO_2 (PCO_2 = 471 Barrer, equivalente a un aumento de 8.5 veces en comparación con el polímero sin modificar) y una selectividad ideal relativamente alta ($\alpha CO_2/N_2$ = 30.2).

El modelado del desempeño de las MMM se llevó a cabo exitosamente mediante el modelo de Maxwell, logrando un buen ajuste incluso para contenidos elevados de ZIF-8 (hasta 60 % vol).

*Trabajo de grado

**Facultad de Fisicoquímica. Escuela de Ingeniería química. Director: Dr Anne Jonquieres, Dr Carlos Jesus Muvdi Nova

Abstract

Title: Synthesis and development of high-performance composite polymer membranes for CO_2 capture*

Author: Maria Valentina Velasco Rueda**

Key words: Polymer, mixed matrix membranes, membranes for carbon capture, PUI, metal organic frameworks

Description: Addressing the challenges of climate change and global warming, membrane separation processes are considered as innovative industrial solutions. Among different membrane materials, mixed matrix membranes are very promising for CO2 capture. In this work, a segmented poly(urea-imide) with high poly(ethylene oxide) content (70 % wt) was selected as a new rubbery polymer matrix and was doped with the metal organic framework ZIF-8.

The new polymer matrix and the optimization of the "priming" method enabled to obtain very high ZIF-8 loadings up to 70 % vol. Various physicochemical methods were used to study the influence of filler/polymer interactions on the membrane's morphology. The CO2 and N2 permeation properties were evaluated by time-lag measurements for both pure gases under standard conditions for CO2 post-combustion capture (2 bar and 35 ◦C).

Very promising membrane performances were achieved for the highest ZIF-8 loading (70 % vol) with a strong increase of the CO2 permeability PCO2 = 471 Barrer (x 8.5 compared to the pristine polymer) and a relatively high ideal selectivity αCO2/N2 = 30.2. The modeling of the MMM's performances was successfully achieved with Maxwell model up to high ZIF-8 content (60 % vol).

*Dissertation

**Facultad de Fisicoquímica. Escuela de Ingeniería química. Director: Dr Anne Jonquieres, Dr Carlos Jesus Muvdi Nova

Introduction

The project aims to analyze the characteristics and separation performances of a series of mixed matrix membranes (MMMs) for carbon capture (CC). The document will be divided into a bibliographic study where the main CC techniques, the different types of membranes used for CC, and their characteristics are compared. A zoom into the MMMs and the various types of fillers used in MMMs will also be explained. Afterward, the methodologies of polymer matrix and MMMs fabrication and characterization are explained. Then, all of the results of the experimental work are presented and analyzed. Moreover, the principle of the permeation measurements and an analysis of the predictive models are explained. Finally, a comparison between the mathematical models and the selectivity/permeability performances of the studied MMMs is carried out before the conclusion and perspectives.

1. Bibliographic study

1.1. Introduction to CO_2 capture and the main related separation processes

The environmental crisis that the planet has been facing since the beginning of the Industrial Revolution has become a priority in the last few years. Changes in temperature, the sea level, acidification in water sources, and so on, have had important consequences including floods, hurricanes, storms, and melting of the polar ice caps, among others. All those natural phenomena have had a great impact on health, the ecosystem, agriculture, and water resources [1,2].

During the Egypt Conference in 2022 (COP27), warnings were again raised because of the increase in global temperature, especially because energy consumption does not seem to diminish, and the primary energy supply is fossil fuels [3]. There are new fossil fuel reserves and, because of the economic growth in developing countries, the energy demand is constantly increasing. In industrialized countries, the energy demand will increase by 0.9% per year, while in developing countries it will increase by 3% [4]. The goal of limiting the temperature rise to 2°C, compared with the pre-industrial era, was reaffirmed in the COP27. However, the temperature of the planet has risen 1.1°C since the industrial revolution [5,6].

The use of fossil fuels for heat and electricity production, transport, and industry, has been identified as one of the main sources of greenhouse gases (essentially carbon dioxide (CO_2), methane (CH_4), nitrous oxides (N_XO), and ozone (O_3)) [7] [2]. The manufacturing sector has been recognized as one of the largest energy consumers and therefore the major producer of CO_2 emissions, representing 64% of the global net anthropogenic greenhouse gases in 2019 [8]. Moreover, Carbon dioxide is accountable for 20% of the thermal absorption in the atmosphere [9].

Due to the environmental effects that the greenhouse gases are causing, different strategies have been developed to mitigate their effects and counter back the environmental crisis nowadays: Technologies for the improvement of the energy efficiency in different equipment, implementation of low or zero-carbon energy, achieve negative CO_2 emissions and stop deforestation [10]. The transition from fossil fuels-based energy production to renewable energies is expensive [11] and time-consuming. Time is not enough to mitigate the effects of climate change; however, the transition is too fast to allow the fossil fuel industry to adapt [12].

CO_2 emissions come mainly from marine bunkers, conventional thermal power, oil and gas pipelines, oil refining, the iron and steel industry, road and air transport, and cement production [5,13]. Carbon

Capture Utilization and Storage (CCUS) is a technology that acts as an emergency solution while the energetic transition is carried out. It is considered economically promising and an asset for industrial effluents that are hard to treat [5,14]. This technology has the potential to be responsible for the reduction of 15% of the cumulative emissions by 2050 [15]. The objective of this technology is to separate carbon dioxide from other gases, capture and store it in geological formations, the oceans, and mineral carbonates, and sometimes, it can be used in enhanced oil recovery and as a feedstock for industrial processes [5,14,16,17]. This technology is classified according to its maturity at the industrial scale. According to Llamas *et al.*, (2012), there are four types [5,14,16,17]:

- Mature Market: Industrial separations, pipeline transport, enhanced oil recovery, and industrial utilization.
- Economically feasible: Post-Combustion Capture, Pre-Combustion Capture, tanker transport, gas and oil fields, and saline aquifers.
- Demonstration phase: Oxy-fuel combustion and enhanced coal bed methane.
- Research phase: Ocean Storage and Mineral Carbonation.

Since the transition to greener energies is going to take time, and society is still going to rely on fossil fuels, then, it is necessary to consider closely Post-Combustion treatment techniques to mitigate the emissions of CO_2 [18]. In Post-Combustion Capture techniques, the carbon dioxide is trapped from the flue gas (mostly carbon dioxide and nitrogen) after the combustion of carbonaceous fuels [14,19]. The main objective of this treatment is to separate CO_2 from N_2. The common conditions of the gas to be treated are moderate temperatures and ambient atmosphere pressure [20]. Figure 1 resumes the most common techniques [21].

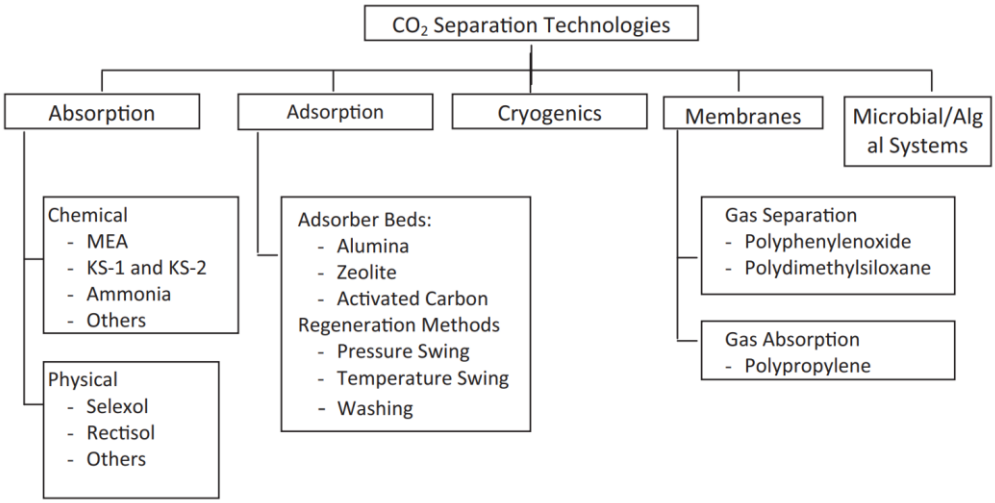

Figure 1. Post Combustion CO_2 Capture techniques. Source: [21]

The absorption processes are divided into chemical and physical absorption. The difference between the two processes is whether the CO_2 reacts with the absorbent (chemical) or not (physical). Usually when a chemical reaction is carried out the speed of absorption is higher. The principle is the same for both techniques. Regarding the first category, amines are a commonly used substance for these purposes; they react in a fast, selectively, and in a reversible way with CO_2 [22].

The flue gas containing CO_2 goes into the absorber column, normally in counter current with the solvent that comes from the stripping unit. The CO_2 is absorbed in the solvent. During the steady process, a gas stream poor in CO_2 is obtained and the rich solvent stream obtained at the outlet of the absorber column is fed into a heat exchanger [22]. For the stripping unit, the opposite procedure is

carried out. Depending on the nature of the liquid solvent and the type of absorption, an inert gas captures the absorbed CO_2 regenerating the solvent that will restart the cycle in the absorber [22].

The entrapment of the CO_2 on a solid surface is called adsorption; different from absorption, which works with a liquid sorbent [23]. This process is also divided into two types: physical and chemical. In the physical process, target molecules get attached to the solid surface by Van Der Walls Forces. This kind of process is usually fast and reversible [24] because of the low heat of adsorption [25]. In chemical adsorption, there is an exchange and transfer of valence electrons between the molecules that are on the solid surface and the molecules that are going to be adsorbed; this generates covalent bonds [25]. This type of adsorption is more selective and allows it to work at high temperatures. Among the most popular adsorbents, there are zeolites, activated carbons and silica [24].

Cryogenic Carbon Capture (CCC) is a technique based on the diminution of the temperature of a CO_2-rich stream until CO_2 solidifies (between -100°C and -140°C). The solid CO_2 is then separated from the light gases [24,26]. The solidified CO_2 can be compressed until the achievement of 100 to 200 times the atmospheric pressure [23].

A membrane for CCS works as a filter; some molecules can pass through it and others do not [20]. This depends on the permeation rates of the species, a parameter that is correlated with the relative size, affinity, and diffusion coefficients of the molecules in the membrane. The driving force in this separation process is the partial pressure difference of the species between the two sides of the membrane [21].

In Table 1 a comparison between the main CC techniques can be found. Nowadays, the main challenge is to find CO_2 capture techniques that are competitive in energy consumption and capital cost [27].

Table 1. Comparison between main CC techniques

Technique	Advantages	Drawbacks
Chemical Absorption with amines	• Amines are cheap [5]. • The process can be carried out even at low CO_2 pressure [5]. • High selectivity. Recovery rates of more than 95% [22]. • Product purity higher than 99%vol can be achieved [22]. • Some of the normally used amines, such as MEA (monoethanolamine) are used because of their high cyclic capacity, their favorable absorption-stripping kinetic rates even with low CO_2 concentrations, and their high solubility in water [5]. • High removal efficiency, stable operation conditions; mature technology background [22]. • Proven technology that is commercially available today [22].	• Amines are highly corrosive, so it is imperative to use equipment made of resistant materials [5]. • Amines react forming stable salts in the presence of O_2, SO_X, particles, HCl, and HF, compromising the composition of the obtained gas [5,22]. • Amine regeneration has high energy requirements that are traduced in high quantities of low-pressure steam and large stripper column reboilers [5,22]. • Amine's degradation [5]. • Need for a large volume of absorbers with expensive packaging to favor the surface mass transfer for the carbon dioxide reaction [22]. • High power loss because of the pressure drops in large absorbers [22]. • Because of the high viscosity of the amines, problems like entraining, channeling, bubbling, and overflowing may occur [22].

		• The need for absorbing and stripping columns represents a high equipment cost [28]. • Foaming in the absorbent column may occur in the presence of heavy hydrocarbons or particles like dust and soot [29].
Absorption using ammonia	• Low heat of absorption compared with amine systems [5]. • Multipollutant control: Absorption of other kinds of impurities that can be found in the gas stream, such as NO, NO_X, and SO_X [5,22]. • High CO_2 transfer capacity [22]. • Lack of degradation during absorption/stripping processes [22]. • Tolerance of oxygen in the treated flue gas [22]. • Stripping steam is not necessary [22].	• The flue gas must be cooled down to 288-300K before it gets in contact with the ammonia. If the change of temperature is not carried out, ammonia can pass to the gas phase (high volatility) [5,22].
Adsorption	• Solid sorbents have low energy requirements compared with the chemical absorption technology [22]. • The implementation of this technology is economically advantageous compared with absorption technologies [22]. • High selectivity, operation simplicity, low cost, ease of regeneration, and low corrosion of the adsorbing material compared with processes that use solvents [28]. • It can be implemented for continuous treatment of the streams [30]. • A large number of available adsorbents [31].	• Only used in high-pressure CO_2 separation [29]. • Pre-treatment stage is necessary (drying and compression) [30]. • If a chemisorption is carried out, heat is required to reverse chemical reactions [32]. • Some adsorbents are sensitive to impurities [31].
Cryogenics	• Allows a high recovery (99.99%) and purity (99.99%) of CO_2 [30,32]. • The cold CO_2 produced can be used as a cold energy source for further industrial applications [30].	• High energy requirements for refrigeration [32]. • Need of water and heavy hydrocarbon removal. If these substances are not removed, they could block the heat exchangers used to diminish the temperature [32]. • It is limited to streams with high CO_2 concentrations, normally more than 50% vol [32], and economically viable from a concentration of 75% [29]. Therefore, this technique is not viable for low-concentrated CO_2 streams, which is normally the case for industrial effluents [32].

Membranes	• Energy-efficient technique [22]. • Polymeric membranes are a competitive option due to their cheap production on a large scale [22]. • A low-cost option for processes that do not require high purity [22]. • Simple modular system [22]. • They do not involve phase changes and they do not need additional separating agents. Therefore, no regeneration treatment [32]. • They involve small carbon footprints compared with other processes [30,32]. The materials that are used for their fabrication and their reduced energy consumption contribute to it. • Membranes require low maintenance [32] because they do not show a fast performance decay. They can be run for long periods without maintenance. If maintenance is necessary, it involves a low cost because, compared with other techniques, it is only necessary to do the membrane replacement. There is no need to replace a large amount of solvent or sorbent [20]. • Modular units that are compact and lightweight, that allow multistage operation [32]. • A membrane system can integrate multiple separations in one unit, for example, the simultaneous removal of CO_2 and H_2S, which would require multi stages systems for other separation processes.	• Some membranes can be plugged by impurities present in the treated gas stream [22]. • Avoiding membrane wetting is complicated [22]. • Low treatment capacity [32]. • Low driving force when treatment of some industrial effluents because of the low partial pressure of CO_2 [29]. • In some cases, the need for energy-consuming compression equipment, has an impact on the economic assessment for industrial-scale applications [24]. • Some membranes are sensitive to corrosive gases, like SO_X, NO_X, and H_2S. In that case, it is necessary to carry out pre-treatment processes for the inlet gas before the membrane treatment [30]. • Some membrane materials are not resistant to practical industry conditions [30]. • If the inlet stream is diluted (less than 20% of CO_2) multistage systems are required [30].

1.2. Introduction to gas permeation

Nowadays, membranes are considered a strong competitor for CCS [14]. However, one of the greatest challenges is achieving simultaneously, high selectivity and permeability [32]. Different models are proposed to describe the permeation process in a membrane. Among the widely used models, there are the solution-diffusion model and the pore-flow model. With the former, the permeants dissolve and diffuse inside the membrane because of the chemical potential gradient [33,34]. A separation between the gases is carried out because of their difference in solubility in the membrane and rate of diffusion [34].

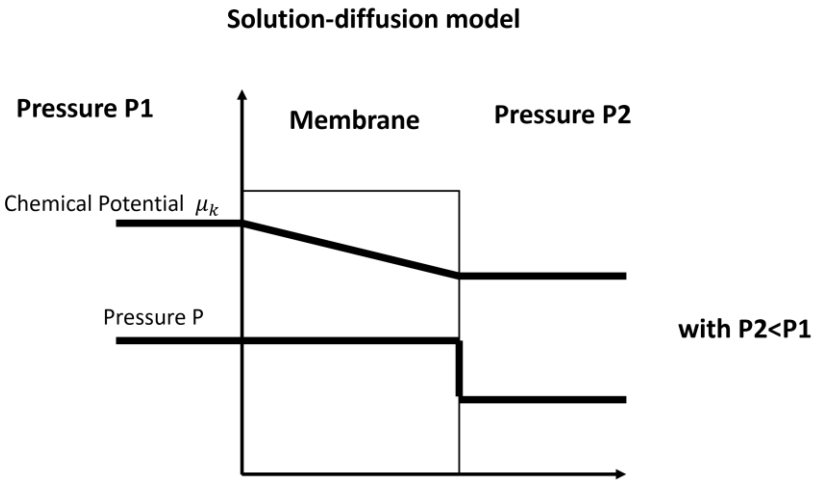

Figure 2. Solution Diffusion model. Adapted from: [33]

The solution-diffusion model considers that the pressure in the membrane is uniform and that the chemical potential gradient is expressed just as a gradient of concentration (Figure 2) [33]. The permeation rate is defined by Fick's law (Equation (1)):

$$J_k = -D_k \nabla c_k \tag{1}$$

Where, $J_k$is defined as the permeation rate, D_k is the diffusion coefficient and c_k is the concentration of the k component in the polymer.

If the equation is integrated between both sides of the membrane, it can be possible to determine the steady-state permeation flux. Considerations such as a constant diffusion coefficient and that Henry's law is applicable are usually made to obtain Equation (2) [35].

$$J_k = \frac{D_k S_k}{e}(y_k P_{k-H} - x_k P_{k-L}) \tag{2}$$

Where $S_k$is the solubility coefficient, e is the active thickness of the membrane, y_k and P_{k-H} are the molar fraction and the pressure in the feed of the k species, respectively. $x_k$and P_{k-L} are the molar fraction of the k species and the pressure in the permeate, respectively [35].

$$\mathcal{P}_k = D_k S_k \tag{3}$$

The product of the diffusion coefficient and the solubility is the permeability $\mathcal{P}_k$ (Equation (3)). According to the nature of the species and the membrane, the permeability can be ruled by the mobility of the molecules dissolved in the membrane (diffusion) or the equilibrium concentration of the dissolved molecules with the gas phase (solubility). Permeability can be expressed in different units, the most widely used is the Barrer, which is also equivalent to $10^{-10}\ N\ cm^3 cm/(s\ cm^2 cmHg)$ [35].

There is another characteristic variable that does not depend on the thickness of the membrane, this is known as the permeation coefficient, and its unit is normally $N\ m^3/(h\ m^2 bar)$ [35].

Permeability is a factor that can be used to measure the performance of the membrane, it describes how easily a molecule can pass through it. Furthermore, there is another parameter that measures the separation quality of the membrane: selectivity $\propto_{k/m}$. The higher the selectivity, the purer the gas. The ideal selectivity is defined as the ratio of the permeability of the two pure gases k and m [34,35].

The selectivity depends on the physicochemical interactions of the molecules present in the gas and the membrane, and how these species can diffuse through the membrane [36].

$$\propto_{k/m} = \frac{\mathcal{P}_k}{\mathcal{P}_m} \quad (4)$$

1.3. Different types of membranes for CO_2 capture

Three main types of membranes have been fabricated for CO_2 separations: ceramic (inorganic), polymeric (organic), and hybrid membranes (a mixture of organic and inorganic). In the industry, it is imperative to operate with materials with high permeability and selectivity to favor the capture of CO_2. Membranes must be thermally and chemically stable, and economically attractive [20].

1.3.1. Inorganic membranes

Some of the inorganic membranes have reached the Robeson 2008 upper bounds (Figure 3); a curve that shows a compromise between the selectivity and the permeability for membrane separation materials and also the zones that are interesting at the commercial scale. This type of membranes is characterized by their thermal and chemical stability, and longer life span (compared with polymeric membranes), which make them suitable for high temperatures and rough conditions. Some of them provide high separation capabilities because of their narrow porous distribution [37–39]. Some others present high permeability, usually, with a decrease in selectivity [40]. However, they usually are brittle, difficult, and onerous to process; most of the time their manufacture involves high temperatures [37,41].

1.3.2. Polymeric membranes

Polymeric membranes are characterized for being operated at moderate temperatures and are easy to manufacture. Moreover, larger surface areas can be achieved; a necessary characteristic for the treatment of CO_2 in the industry. They have mechanical properties that surpass those of the inorganic membranes [14,27]. Nevertheless, the swelling and plasticization that CO_2 can trigger into the membrane is something that has to be solved [27], in particular for gas feeds with high CO_2 partial pressure.

CO_2 is a gas that can diffuse rapidly in a wide range of membrane materials, including rubbery and glassy polymers [32]. Since the kinetic diameter of CO_2 is smaller than N_2 (3.3 A for the former, 3.64 A for the latter), the former always has a bigger diffusivity inside the membranes [20]. Liu et al., (2012) affirmed that CO_2 has a relatively high molecular weight and a large quadruple moment, enabling it naturally to adsorb more strongly in polar membrane materials compared to other gas species [32]. Different types of polymers such as polyacetylenes, polyacetates, polyaniline, polyetherimides, tetramethyl hexafluoro bisphenol-A polycarbonate (TMHFPC), polysulfones, polyimides, polyetherimides, polycarbonates, poly (phenylene oxide), poly(ethylene oxide), polyacrylate and poly sulfone have been studied for Post Combustion CC [20,27,41].

The study of the performance of many homopolymeric membranes has been carried out, and the trade-off phenomenon between selectivity and permeability was generally observed (Robeson upper bound) [42,43]. Research is focused on producing membranes that surpass the upper bound, which was updated by Robeson in 2008 (Figure 3) [44]. It has been proven that polymer mixes, cross-linked polymers, and copolymers are a potential solution for overcoming the trade-off phenomenon; problems that a single polymer presents can be compensated, and the different advantages offered

by different types of functional groups can be combined [27]. Among the solutions that have been analyzed to improve the performance of the polymer membranes include:

- Incorporation of flexible and polar groups into the polymeric membrane [32]. These groups have a strong affinity with CO_2 because of the dipole interactions [45].
- Use of soft segments inside of the polymeric chains [32].
- Modification of block copolymers, enhancing the physical cross-linking, to achieve the desired mechanical properties [32].
- Increase the free volume of the membrane by adding nanoparticles [32].
- Polymer blending and interpenetrating polymer networks [32].

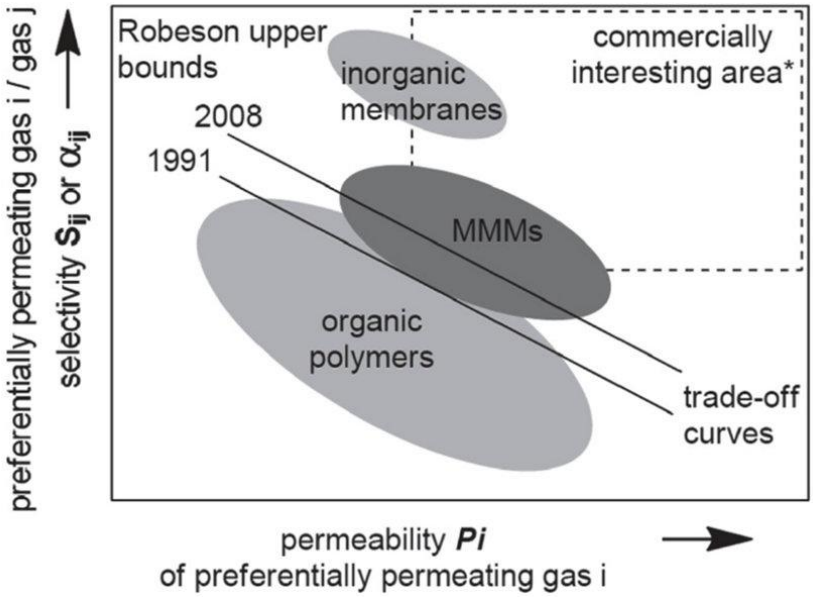

Figure 3. Robeson upper bound. Source: [46].

According to Han et al., (2021) polymers containing ethylene oxide (EO) units, polymeric ionic liquids, the perfluoropolymers, thermally arranged polymers, and glassy polymers with triptycene as building blocks are widely used and interesting options for CC[19].

The oxyethylene-rich rubbery polymers showed great performance for CO_2 separation and interaction of high specificity with this molecule compared with other gases [27,45]. Carbon dioxide has an affinity with the ether group because of the quadrupole-dipole interactions. Specifically, poly(ethylene oxide) (PEO) has shown a high affinity with CO_2. Besides the characteristics mentioned before, the oxygen of the ether group has a rotation ability that concedes flexibility to the polymeric chain; this favors the fraction of free volume in the membrane. Nevertheless, because of its weak cohesive energy if the molecular weight is low, PEO will not form a steady membrane. If there is a high molecular weight, it will tend to crystalize [45] because the flexible ether will form linkages [19] affecting the permeation properties. To diminish these effects, copolymerization with rigid segments, blending with polymers with a lower molecular weight, and triggering the formation of secondary polymer chains by cross-linking or branching have been done [19,45].

In the case of PEO, copolymerization with rigid segments has been a good approach [19]. PEO has the function of the separation of gases, because of its affinity with CO_2, while the rigid segments provide mechanical properties for the membranes, can increase the free volume, and disrupt the chain packaging; avoiding the crystallization of the PEO [19]. The rigid segments can be made of polyamide,

polyimide, and polyester [45]. The transport properties of gas in the polymer can be controlled by the crystallinity and the content of EO groups in the chains. The objective is to have as many as possible of EO groups in the final product without triggering crystallization in the material, which would compromise permeability and selectivity [47].

Over time, different kinds of PEO copolymers have been synthesized: Pebax, Polaris, Polyactive, and poly(ether-urea-imide), among others [27,42]. The former is a thermoplastic elastomer that is made of polyamide rigid segments and polyether flexible segments (poly(ethylene oxide). The latter is a copolymer developed by Solimando *et al.*, (2017) at the LCPM (Laboratory of Macromolecular Physical Chemistry), outstanding because of their film-forming properties, high selectivity, and improved physical cross-linking by the hard-aromatic blocks, which enhances the mechanical properties of the material. Also, it has good adhesion with different supports [42]. The soft blocks are made of Jeffamines (which are short oligomers with oxyethylene and oxypropylene monomer units) and the hard blocks are made of urea-imide. The authors carried out different experiences to define the optimal content in soft blocks and hard blocks, varying the weight percentage of soft blocks from 41 to 70 %. They concluded that the copolymer with the highest percentage of soft blocks (PUI JFAED 2000) had the best permeability/selectivity performances among the different copolymers that were studied. Figure 4 shows the arrangement of the soft blocks/hard blocks of the copolymers, with their soft block percentage and permeability.

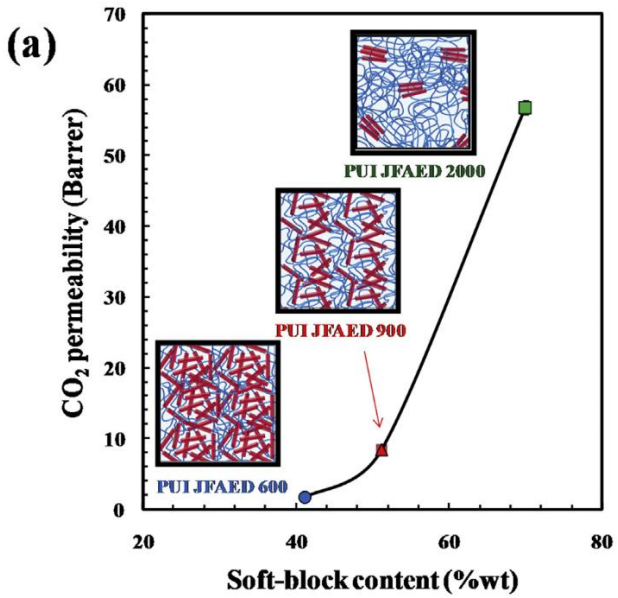

Figure 4. Poly(ether-urea-imide) morphology with different soft block weight percentages and their permeabilities. Source: [42]

1.3.3. Mixed Matrix Membranes (MMMs)

Despite the technological improvements that have been developed regarding the structure and morphology of the polymers, a higher CO_2/N_2 selectivity is required to obtain materials that can compete with the other CC technologies at the industrial scale. To take advantage of the interesting characteristics of organic and inorganic materials, and cancel the disadvantages that they can present, mixed matrix polymeric membranes (MMMs) have become an interesting alternative, providing enhanced separation properties while maintaining acceptable flexibility of the matrix [36]. A MMM is made of a polymeric continuous phase where an inorganic or hydride material is dispersed as a filler [41,43] (Figure 5). The organic and dispersed phases must be selective for the same gas pairs [36]. The presence of the fillers in the membrane ameliorates permeability due to their molecular sieving effect

and creation of free volume [38], however, it is necessary to find a compromise between these effects to maintain selectivity. MMMs carry out the separation by size selection between the molecules present in the gas to treat or by selective transport according to the difference in solubility of the gas molecules in the membrane [36]. Among the advantages of MMMs, it can be found enhanced mechanical and thermal stability compared with simple polymer membranes, their separation performance is higher than simple polymer membranes and the plasticization phenomenon can be reduced due to the hardening of the polymer matrix by the filler particles [38]. Table 2 summarizes the main properties of the MMMs, polymeric and inorganic membranes, showing that MMMs provide a good compromise between all of the relevant properties for CC.

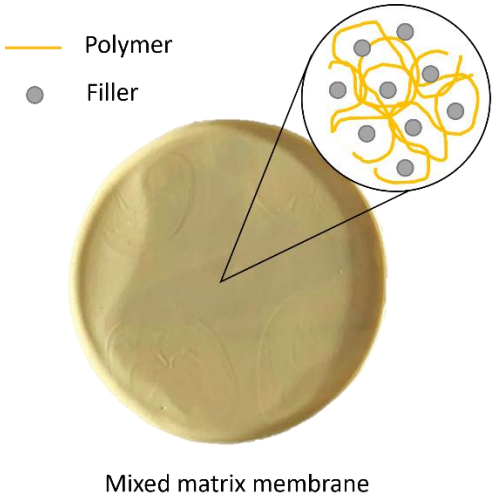

Figure 5. Structure of a mixed matrix membrane

Table 2. Properties comparison of MMMs, polymeric and inorganic membranes. Source: [48]

Properties	Polymeric membranes	MMMs	Inorganic Membranes
Separation Performances	Low to moderate	Moderate	High
Chemical and Thermal Stability	Moderate	Excellent	Excellent
Mechanical Strength	Excellent	Good	Poor
Fabrication Cost	Low	Moderate	High

MMMs can be classified into two groups depending on the type of fillers added to the matrix. If the filler is porous, then the selectivity for small gas molecules can be enhanced because the size exclusion effect increases, or because the nanopores have a good affinity towards the gas molecules [41]. On the other hand, if the filler is nonporous, it modifies the molecular packing of the polymer chains [36], then the free volume of the membrane can increase and consequently its permeability.

The major factors that can influence the MMM's performances are the type of filler and polymer, the combination and interaction between these two (morphology of the interface), the size and texture properties of the filler [36,38], the interactions between the gas and the membrane [38], and the fabrication process [41,43]. Among the commonly used fillers, zeolites, carbon molecular sieves, 0-D carbon quantum dots, 1-D carbon nanotubes, activated carbon, non-porous-silica, C_{60}, graphite, metal oxides nanoparticles, and Metal-Organic Frameworks (MOF) can be found [36,38,41,43]. The latter are hybrid materials with a porous crystalline structure composed of metal centers linked between each

other by organic ligands [49,50]. They have been considered an interesting choice for MMMs because of the high surface area that they provide (because of their high porosity), availability in different types and shapes, their tunable pore/channel sizes, and good compatibility with the several polymer matrices because of the presence of organic linkers (which reduces the non-selective defects at the MOF-polymer interface) [41,43,49,51].

MMMs, in which MOFs are used as fillers, have recently been studied to overcome the permeability-selectivity trade-off and surpass the upper boundary of Robeson's curve. The chemical structure and the functional groups that are on the surface and affect the interaction with the polymer matrix are relevant factors for the appropriate dispersion of the MOF fillers [43]. The surface of MOFs can be treated to have suitable chemical functionalities that reduce the formation of microvoids between the organic and the inorganic phases; this is traduced in the minimization of selectivity loss [43]. Also, it is important to use a specific kind of MOF depending on the type of separation that must be carried out. According to Li et al., (2021), the MOFs that have been used for carbon capture in recent years are: x-UiO-66, x-MIL-53, and, ZIF-8, where x is a functional group [41]. The structure-property relationships demonstrated that MOFs with small pores and moderate porosities can lead to MMMs with high CO_2 selectivities [31].

Zeolitic imidazole frameworks (ZIFs) are an attractive category of MOFs. They are composed of metal nodes, usually of Zn, that are interconnected with imidazolate linkers, this allows to adopt different kinds of 3-D structures [41,52]. ZIF-8 (Figure 6) has been deeply studied for CO_2 separation because its pore size is around 3.4 A°, which is approximately the same value of the kinetic diameter of CO_2: 3.3A°. Also, it is highly thermally and chemically stable [53].

In Table 3, examples of MMMs from the literature for CO_2/N_2 separation are presented. For almost all of the data, the measurement conditions (pression and temperature) were of the same order of magnitude. Zheng et al., (2019), carried out a study comparing the permeability and selectivity of the membranes changing the size of the ZIF-8 nanoparticles dispersed in a PEBAX- MH1657 matrix. They concluded that the addition of the different-sized fillers gave an improvement in permeability compared with the free-filler membrane. However, when the charge of the filler increased, the CO_2/N_2 selectivity was compromised. They justify this phenomenon by explaining that in these cases, microphase separation started to appear, enhancing N_2 permeability [53]. This phenomenon can be also seen in the study of Murali et al., (2014), a direct augmentation of permeability with the increase of charge load, but a correlated loss of selectivity [54]. Among the presented MMMs, the polyActive MMM by Lee et al., (2021) [55] showed high values of carbon dioxide's permeability and selectivity, demonstrating an optimal compromise between these two properties. Regarding the MMMs fabricated with PEBAX-1657 as the polymer matrix, with the ZIF-8 as a filler, higher values of carbon dioxide's permeability were obtained compared with the values obtained when the fillers were UiO-66. Nevertheless, higher values of selectivity were registered with the UiO-66 because of the better selectivity of that particular filler.

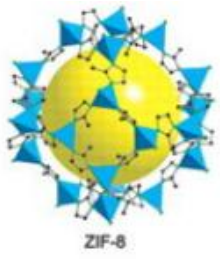

Figure 6. ZIF-8 3D structure. Blue: Zinc atoms. Black: Imidazole functions. Source: [41]

Table 3. Examples for MMMs based on of different fillers for CO_2/N_2 separation.

Polymer Matrix	Filler	T °C	Feed Pressure (bar)	Thickness (µm)	Single/Mixed gases	P CO_2 (Barrer)	P N_2 (Barrer)	$\propto_{CO_2/N_2}$	Ref
PEBAX-MH1657	ZIF-8-90nm (5wt.%)	20°C	1	-	Mixed	99.7	1.67	59.6	[53]
PEBAX-MH1657	ZIF-8-90nm (20wt.%)	20°C	1	-	Mixed	156.2	3.86	40.5	[53]
PEBAX-1657	ZIF-8@CNTs (5wt%)	35°C	5	80-100	Mixed	≈225	≈ 4.6	≈ 49	[56]
PEBAX-2533	ZIF-8@GO (6wt%)	25°C	1	-	Mixed	249	5.2	47.6	[57]
PEBAX-1657	Zeolite 4A (5wt.%)	T amb	4.9-24.5	-	Single	71.4 ± 5.1	1.4 ± 0.1	52.8 ± 3.1	[54]
PEBAX-1657	Zeolite 4A (10wt.%)	T amb	4.9-24.5	-	Single	97.0 ± 4.9	1.8 ± 0.1	54.0 ± 2.5	[54]
PEBAX-1657	Zeolite 4A (20wt.%)	T amb	4.9-24.5	-	Single	113.7 ± 5.5	2.9 ± 0.2	39.5 ± 1.5	[54]
PEBAX-1657	Zeolite 4A (30wt.%)	T amb	4.9-24.5	-	Single	155.8 ± 6.9	12.0 ± 1.0	12.9 ± 0.5	[54]
PEBAX MH 1657	ZIF-300 (30wt.%)	20°C	4	-	Single	≈83	0.98	≈85	[58]
PEBAX-MH 1657	GO (0.1wt.%)	25°C	3	-	Single	≈95	1.1	≈83	[59]
PEBAX-MH 1657	UiO-66-NH_2(7.5wt%)	20°C	3	-	Single	≈ 78	1	≈ 76	[49]
PEBAX-MH 1657	UiO-66-NH_2(10wt%)	20°C	3	-	Single	≈ 82	1	≈ 79	[49]
PEBAX-MH 1657	UiO-66-NH_2(7.5wt%)	20°C	3	-	Mixed	≈ 80	1.4	≈ 58	[49]
PEBAX-MH 1657	UiO-66-NH_2(10wt%)	20°C	3	-	Mixed	≈ 84	1.3	≈ 63	[49]
PolyActive	P@MOF2 (40wt%)	35°C	3	90-120	Single	425	7.61	56	[60]
PEGDA	UiO-66(20 wt%)	35°C	1	170-230	-	470	11.5	41	[55]
Matrimid	ZIF-8 (30wt.%)	35°C	2.7	-	Single	14.23	0.59	24	[61]
Matrimid	ZIF-8 (40wt.%)	35°C	2.7	-	Single	24.55	1.05	23.4	[61]
Matrimid	ZIF-8 (50wt.%)	35°C	2.7	-	Single	4.72	0.18	26	[61]
Matrimid	ZIF-8 (60wt.%)	35°C	2.7	-	Single	8.08	0.44	18	[61]

1.3.4. Models for permeability prediction of MMMs

Different models have been developed to predict MMMs performances and to establish a comparison between the experimental data. This comparison allows to have a better understanding of the properties-structure relationship of the MMM. According to Keskin et al., (2019), the predictive models can be classified into three categories: Resistance based models, simulation-based rigorous models, and effective-medium theory-based models. For the first category, the transfer in the membrane is understood as an electrical circuit composed of numerous layers of filler and polymer, where the gas flow can be parallel or in series to the two phases. In this category of models, the fillers are considered cubic particles regularly dispersed in the polymer matrix [62]. The second one provides, at the

nanoscale, the possible relationship between the polymer and the fillers, providing information about the structures and properties of the MMM [63].

For the effective medium theory models, the volume fraction of fillers and the permeability of each phase are considered. This category is divided into two groups: the ideal and non-ideal models. The former considers that the membrane is composed of two phases (the polymer and the fillers) with ideal contact between both and no defects in the interface [62,64,65]. It is the simplest approach and the one commonly used in the literature, as the information required to analyze these models is readily available. Among the well-known models that belong to this category, it can be found: the Original Maxwell model and the Bruggeman model which consider the particles as perfect spheres randomly dispersed in the matrix [62]. Also, some ideal models consider the distribution, shape, or aggregation of the fillers, like, Lewis-Nielsen, Pal Cussler, Gonzo-Parentis-Gottifredi, Kang-Jones-Nair, the generalized Maxwell model, and Maxwell-Wargner-Sillar. In the frame of this project, only the ideal models will be presented in detail (Maxwell, Bruggeman, Pal, and Lewis-Nielsen).

In Table 4, a summary of the models that are used in this study for the prediction of the performance of the ZIF-8/PUI MMMs is presented. Since carbon dioxide and nitrogen will be studied separately, the permeability will be calculated for the pure gases. The employed nomenclature is described below:

- P_{eff} describes the effective steady state permeability of the MMM [64].
- P_c corresponds to the permeability of the continuous phase.
- P_d corresponds to the permeability of the fillers (dispersed phase).
- φ_d corresponds to the filler volume fraction in the MMM.
- λ_{dc} is the ratio between the permeability of the dispersed and continuous phases [66]. $\lambda_{dc} = \frac{\mathrm{P}_d}{\mathrm{P}_c}$
- P_r is the reduced permeability of the MMM. It's the ratio between the effective permeability and the permeability of the continuous phase. $\mathrm{P}_r = \frac{\mathrm{P}_{eff}}{\mathrm{P}_c}$
- G geometric factor shape of the dispersed phase [67].
- n is a shape factor of the filler [68].
- φ_m represents the maximum packing volume fraction of filler particles.

The meaning of φ_m is similar to the atomic packing factor (APF) for crystallographic cells, represented by Equation (5):

$$APF = \frac{N_{atoms} V_{atom}}{V_{unit\ cell}} \tag{5}$$

N_{atoms} is the number of atoms in the cell, V_{atom} the volume of one atom and $V_{unit\ cell}$ the volume of the cell. In the case of the MMMs, the atoms are represented by the fillers. Since the models that use φ_m consider the particles as spheres, the volume of one particle will correspond to the volume of a sphere. For a simple cubic cell, the packing factor is 0.68 and for a body-centred cubic cell, the packing factor is 0.52 [69]. The considered value of 0.64 is between the values presented before, ensuring that the analogy with the packing factor is coherent.

Table 4. Ideal models for MMMs used for this study

Category	Model	Description	Equation	Restrictions and considerations
Ideal Models that do not consider the size and distribution of the fillers	Maxwell [64]	The Maxwell model was created to calculate the electrical conductivity of particles infinitely diluted in a matrix [70]. Afterwards, it was used to estimate MMMs performance at low filler volume fraction [62].	$\mathcal{P}_{eff} = \mathcal{P}_c \frac{\mathcal{P}_d + 2\mathcal{P}_C - 2\varphi_d(\mathcal{P}_c - \mathcal{P}_d)}{\mathcal{P}_d + 2\mathcal{P}_C + \varphi_d(\mathcal{P}_c - \mathcal{P}_d)}$ (6)	• The MMM must have less than 0.2 volume fraction of filler [66,71], for higher values, the model is not accurate to predict the permeability of the MMMs [64,66]. • It is necessary to consider that the distance between the filler particles is large enough to ensure that the gas flow is not disturbed by the presence of other particles in the matrix [72]. • The model does not contemplate the effects of the particle size, shape and aggregation of the particles [64,65]. • This model tends to underestimate the permeability for high values of φ_d[66]. • Explicit relationship, therefore easy to solve [66].
	Bruggeman [64]	It was originally developed to predict the electric constant of particle composites. It's considered as an improvement of Maxwell's equation [64].	$\mathcal{P}_r^{\frac{1}{3}}\left(\frac{\lambda_{dc} - 1}{\lambda_{dc} - \mathcal{P}_r}\right) = (1 - \varphi_d)^{-1}$ (7)	• It considers systems with a larger amount of spherical filler particles distributed randomly in the matrix, compared with the Maxwell's model [64]. However, when φ_d is close to φ_m significant deviations are expected [66]. • All the other Maxwell's limitations still apply [64].

Ideal Models that consider the size or distribution or aggregation of the particles	Lewis-Nielsen [64]	The model was conceived to estimate the elastic modulus of spherical particulate composites [65,73].	$$\mathrm{P}_r = \frac{1 + 2\left[\frac{\lambda_{dc} - 1}{\lambda_{dc} + 2}\right]\varphi_d}{1 - \left[\frac{\lambda_{dc} - 1}{\lambda_{dc} + 2}\right]\varphi_d \psi} \quad (8)$$ Where ψ is the Lewis Nelson correction factor [74]: $$\psi = 1 + \left(\frac{1 - \varphi_m}{\varphi_m^2}\right)\varphi_d \quad (9)$$	• This model considers morphological characteristics of the filler using the φ_m parameter. This parameter is affected by the size and shape of the fillers, as well as the aggregation of them [65]. • It represents a correct prediction for values between 0< φ_d<φ_m [64]. • Explicit relationship, therefore easy to solve [66].
	Pal [64]	This is one of the most recent models, developed to estimate the thermal conductivity of particulate composites and then adapted for the prediction of the permeability [75].	$$\mathrm{P}_r^{\frac{1}{3}}\left(\frac{\lambda_{dc} - 1}{\lambda_{dc} - \mathrm{P}_r}\right) = (1 - \frac{\varphi_d}{\varphi_m})^{-\varphi_m} \quad (10)$$	• It considers the packing difficulty of the filler [64]. • It considers the morphology of the particles as a function of φ_m[64]. • It covers a wide range of particles volume fraction, between 0< φ_d<φ_m [64]. • When φ_m is close to one, this model becomes Bruggeman model.

1.3.5. Permeation Theory

The time-lag method consists of the exposure of a membrane, which is free of any dissolved gas, to a sudden (so-called Dirac step) increase of pressure at the upstream side of the membrane, while the other side (downstream) is initially under vacuum [77] (around 0.02-0 mbar in the case of the study). Because of the solution-diffusion gas permeation phenomena, the gas molecules will dissolve into the MMM, then they will diffuse in it, to finally reach the opposite side of the membrane, where the pressure is measured. After the Dirac step, the upstream pressure (P1) is supposed to be constant all over the measurement. Downstream pressure (P2) is registered over time. This method allows to have a direct determination of the permeability and diffusion coefficient and then, a deduction of the solubility coefficient (Equation (3)) [78].

Permeability determination

The gas permeation process is divided into two: the transient and the steady state phases. For both, diffusion is the limiting step. The flux of gas follows the first Fick's law (Equation (1)). Making the hypothesis that the system follows Henry's law for polymer sorption, Equation (11) is obtained.

$$c = S_K \mathcal{P}_K \tag{11}$$

Also considering Equation (3), Equation (1) becomes Equation (12). n_{gas} corresponds to the gas moles that flow during a t time. A is the membrane surface and l is the membrane thickness. In the international system of units, the flux will be in mol*m^{2}*s^{-1} and the permeability mol*m*m^{-2}*s^{-1}*Pa^{-1}.

$$J_K = \mathcal{P}_K \frac{(P_1 - P_2)}{l} = \frac{n_{gas}}{At} \tag{12}$$

Since the downstream is supposed to be under vacuum, the value of P2 can be neglected compared to P1. Then, by considering that the gas molecules are responsible for the increase in the downstream pressure in the steady state, Equation (12) can be expressed as Equation (13), where V_2 is the downstream volume. $\left(\frac{dP_2}{dt}\right)_{Steady\ state}$ corresponds to the slope of the linear regression obtained with the time and downstream pressure in the steady state. $\left(\frac{dP_2}{dt}\right)_{Leaking\ rate}$ corresponds to the slope of what is identified as the leaking rate. The latter is considered in the equation because possible leaks in the system can modify the outcomes of the measurement. Usually, the leaking rate is very low. For good data analysis, it should be at least a hundred times lower than the slope of the permeation curve in the steady state. This is normally easy to achieve for gases with high permeability, but it can be more difficult for slowly permeating gases (like nitrogen for membranes of interest in this work). Therefore, the leaking rate should not be neglected for low-permeating systems [65]. We considered it systematically for CO_2 and N_2 in this work.

$$\mathcal{P}_K = \frac{n_{gas} l}{A t P_1} = \frac{V_2}{RT} \frac{l}{A P_1} \left(\left(\frac{dP_2}{dt}\right)_{Steady\ state} - \left(\frac{dP_2}{dt}\right)_{Leaking\ rate} \right) \tag{13}$$

If the international system was used for the Equation (13), the permeability in Barrer ($\mathcal{P}_{KB}$) is obtained with the Equation (14) [78].

$$\mathcal{P}_{KB} = 2.953 * 10^{15}\, \mathcal{P}_K \tag{14}$$

Determination of diffusion coefficient and sorption coefficient

The diffusion coefficient is determined from the time-lag (θ), which is defined as the intercept between the leaking rate straight line and the steady state straight line (Figure 7). According to the literature and as explained before, the slope of the steady-state curve should be at least 100 times bigger than the leaking rate curve [78]. Note that the steady state is obtained after a time equal to 5θ and for calculating the slope of the steady-state regime, we made a linear regression of the data obtained in the time range of 5θ to 10θ.

With Equation (15) the diffusion coefficient is determined, and with Equation (3), the solubility coefficient is obtained as the ratio of permeability and diffusion coefficient.

$$\theta = \frac{l^2}{6D} \tag{15}$$

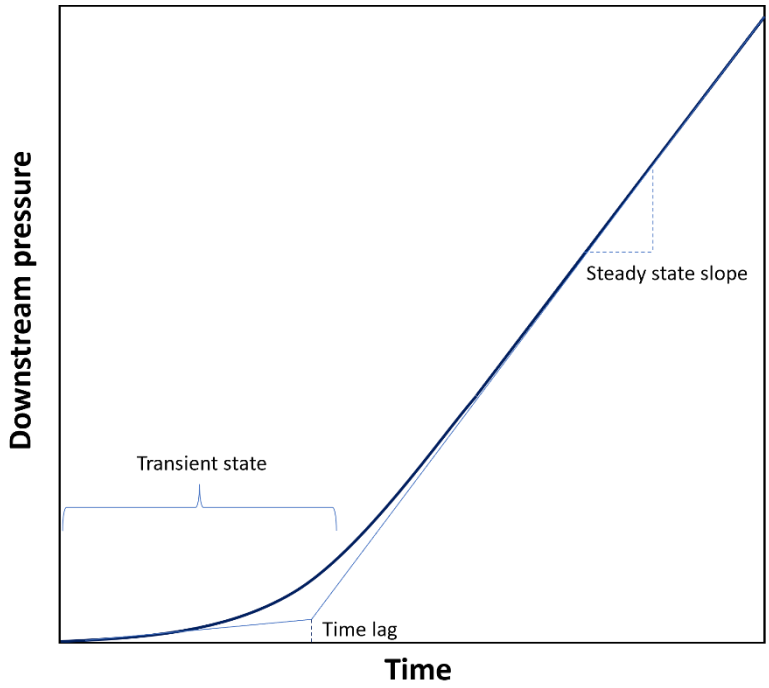

Figure 7. Time-lag determination

1.4. Conclusion of the bibliographic study and introduction to the Master Project

The addition of MOFs into a polymer matrix is much easier to achieve on the industrial scale than the production of inorganic-hybrid membranes because traditional techniques for polymer synthesis can be used [51]. Nevertheless, there are some drawbacks concerning the implementation of this technology. In the first place, achieving the fabrication of MMMs where the fillers are well dispersed and compatibilized is challenging. Moreover, the performance of the recent membrane technologies does not surpass the performance that conventional CO_2 extraction technologies can offer. Additionally, there is not a full understanding of the mechanism of separation in these membranes at the microscopic scale, therefore it is still difficult to predict or propose a refinement of the already proposed mechanisms [55].

The objective of this project is to evaluate the performance of a series of novel Mixed Matrix Membranes (MMMs) for post-combustion carbon capture, specifically focusing on the CO_2/N_2 separation process. The study was based on the most effective copolymer synthesized by Solimando *et al.* (2017) in a previous LCPM study on PEO-based poly(urea-imide) (PUI JFAED 2000), which has been previously introduced.

The ZIF-8 filler was selected for the development of the new MMMs due to its high CO_2 permeability, its well-documented performance reported in the literature, as well as its optimal particle size and large-scale commercial availability from BASF. In this study, membranes incorporating ZIF-8 filler in quantities ranging from 10% to 70% vol/vol was analyzed to investigate the effect of filler content on membrane performance.

The PUI 2000 has already shown high performances for CO_2 capture, corresponding to a permeability of 57 Barrer and a selectivity CO_2/N_2 of 50 (measures carried out with a feed pressure of 2 bar and at 35°C) [42]. The objective of the project is to obtain new Mixed Matrix Membranes expecting even higher performances (selectivity and permeability) than the single polymer matrix.

In this document, the methodology and results for each objective are presented together for clarity.

GENERAL OBJECTIVE

Study the separation performance of CO_2/N_2 of the PEO-based poly(urea imide)(PUI JFAED 2000) MMMs with ZIF-8 as the filler.

SPECIFIC OBJECTIVES

- Elaborate Mixed Matrix Membranes (MMMs) with potential for carbon capture and perform their physicochemical characterization.
- Conduct permeation measurements to obtain CO_2 and N_2 permeability, as well as CO_2/N_2 selectivity.
- Compare the experimental data with the theoretical values calculated using predictive models.

2. Methodology and results

2.1. 1ST Objective: Elaborate Mixed Matrix Membranes (MMMs) with potential for carbon capture and perform their physicochemical characterization.

2.1.1. Methodology

2.1.1.1. Polymer

2.1.1.1.1. Polymer synthesis

The reaction scheme is based on the synthesis of Solimando et al., (2017) (Figure 8). The synthesis of the PUI copolymer is a polycondensation from a macro-diisocyanate. In the first step, the terminal amine groups of the Jeffamine diamine oligomer reacted with the NCO terminal groups of the aromatic diisocyanate (MDI). This reaction gives as a result a micro-diisocyanate. As a second step, a chain extension is carried out by adding the 6-FDA. This reaction is catalyzed by the triethylamine. As a secondary product of this reaction, carbon dioxide is obtained. To finally obtain the PUI, the thermal cyclization triggered the reaction between the amine and acid groups, giving as a result the imide and water, as a secondary product. This synthesis allowed the obtention of UI hard blocks with strong physical crosslinking interactions, improving the mechanical properties of the material [42].

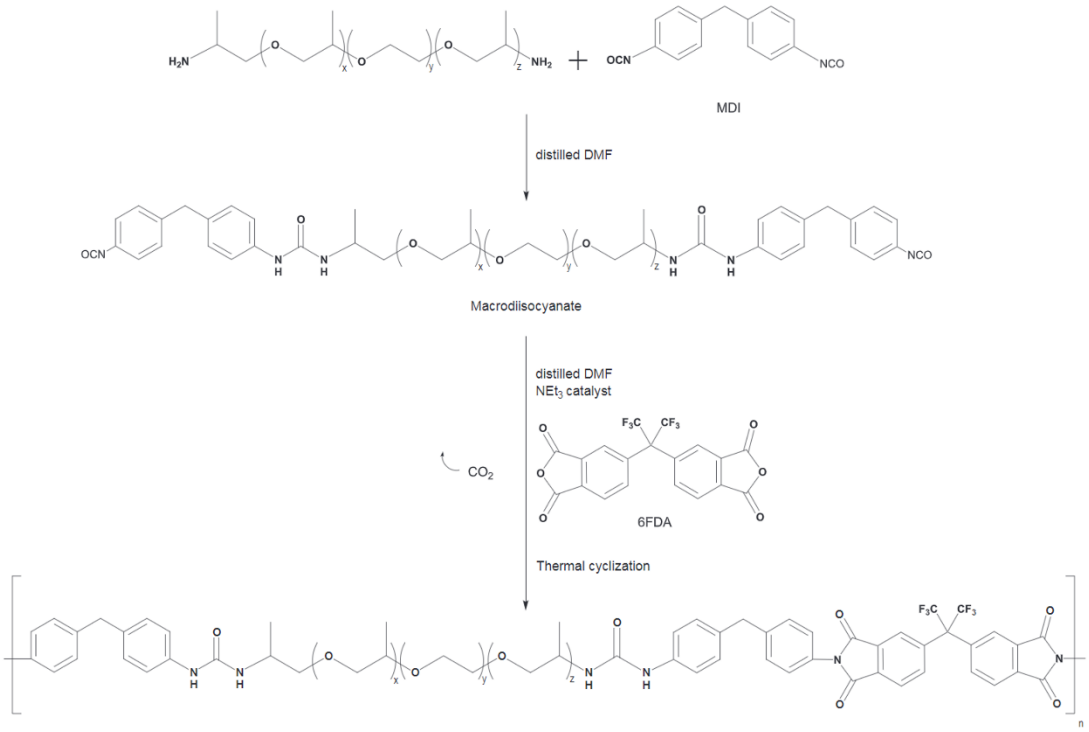

Figure 8. Reactions for linear PUI synthesis. Source: [42]

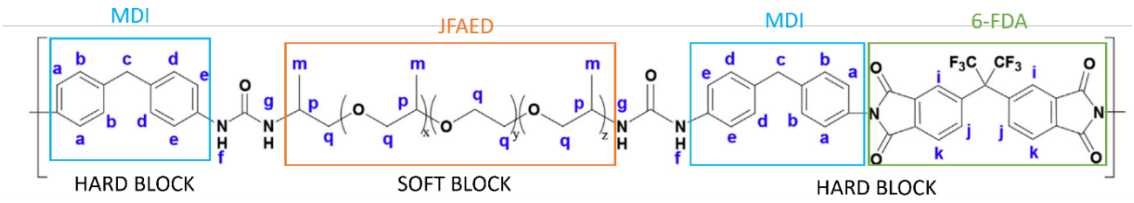

Figure 9. Linear PUI structure. Adapted from: [42]

Table 5. Solvents, reagents, and catalyst for PUI and membrane syntheses

Substance	Function	Purification	Stocking
Jeffamine (JFAED 2000)	Reagent	Vacuum drying at 40°C.	Under dehydrated argon and at 4°C
Methylene diphenyl diisocyanate (MDI)	Reagent	Vacuum distillation at 175°C.	Under dehydrated argon and at -20°C
4,4'-(Hexafluoroisopropylidene)diphthalic Anhydride (6-FDA)	Reagent	Vacuum sublimation at 225°C	Under dehydrated argon and at room temperature
***N, N*- Dimethylformamide (DMF)**	Solvent	Fractional distillation under vacuum over calcium hydride at 40°C.	Under dehydrated argon, activated molecular sieve at room temperature.
Chloroform	Solvent	-	At room temperature
Triethylamine (Net_3)	Catalyst	Distillation over KOH at 90°C.	Under dehydrated argon, molecular sieve at room temperature.

Before starting the PUI copolymer synthesis, it was necessary to define the masses of the different reagents JFAED 2000, MDI, and 6-FDA corresponding to the target stoichiometry as shown in Table 6. The real number-average molar mass of the employed Jeffamine is 2102 g/mol (as formerly determined at LCPM by titration of its amine end groups), however, it will be called JFAED 2000, which refers to its commercial name.

Table 6. Molar masses and stoichiometry of reagents

Reagent	Molar mass (g/mol)	Equivalents in the repeating motif
JFAED 2000	2102	1
MDI	250.25	2
6-FDA	444.24	1

Taking as a calculation basis 5 g of JFAED 2000, the quantity of MDI and 6-FDA is determined as follows:

$$\boldsymbol{mols\ of\ JFAED} = 5\ g\ JFAED * \frac{1}{2102\ \frac{g}{mol}} = 2.38 * 10^{-3}\ mol\ JFAED$$

$$\boldsymbol{MDI\ mass} = 2.38 * 10^{-3}\ mol\ JFAED * \frac{2\ mol\ MDI}{1\ mol\ JFAED} * \frac{250.25\ g\ MDI}{mol\ MDI} = 1.1905\ g\ of\ MDI$$

$$\boldsymbol{6-FDA\ mass} = 2.38 * 10^{-3}\ mol\ JFAED * \frac{1\ mol\ 6-FDA}{1\ mol\ JFAED} * \frac{444.24\ g\ 6-FDA}{mol\ 6-FDA} = 1.0567\ g\ of\ 6-FDA$$

The synthesis of the PUI copolymer was carried out over a five-day period. On the first day, Jeffamine 2000 was removed from the refrigerator and MDI from the freezer at the end of the day, allowing both reagents to return to room temperature overnight.

On the second day, approximately 5 g of Jeffamine 2000 were weighed and dissolved in 15 mL of anhydrous DMF under stirring and a dry argon atmosphere. Full dissolution was achieved within 3–4h. Based on the exact Jeffamine mass, the required amounts of MDI (approximately 1.19 g) and 6-FDA (approximately 1.06 g) were recalculated. The MDI was weighed in a separate flask and then added to the Jeffamine solution. The mixture was stirred under argon at room temperature for 3 h. Subsequently, 45 mL of DMF and five drops of triethylamine were added, followed by the gradual addition of 6-FDA under inert conditions. The temperature was increased to 60 °C and maintained for 1.5 h, then raised to 80 °C for 8 h. To prevent pressure buildup from CO_2 evolution, the reaction flask was kept slightly open.

On the third day, the reaction mixture was concentrated using a rotary evaporator and precipitated in water under vigorous stirring to form a vortex. Once precipitation began, the mixture was filtered and the polymer was transferred into Teflon molds. This process was repeated until the full solution was processed. The molds were left overnight under a fume hood to remove residual water.

On the fourth day, the polymer was further dried in a vacuum autoclave at 60 °C for 6 h, with the liquid trap cleaned during the process. The temperature was then increased to 130 °C and maintained overnight to promote thermal cyclization of the imide rings.

On the fifth day, the resulting polymeric films were de-molded and collected for further use.

2.1.1.1.2. Characterization of the polymer

- Polymer yield

To evaluate the performance of the polymer synthesis, the following equations are used:

$$\boldsymbol{Theoretical\ polymer\ mass} = Experimental\ JFAED\ (g) * \frac{mol}{2102\ g} * \frac{2958\ g\ repeating\ motif}{mol} \quad (16)$$

$$\boldsymbol{Yield} = \frac{Experimental\ polymer\ mass}{Theoretical\ polymer\ mass} * 100\% \quad (17)$$

The experimental moles of the JFAED 2000 were calculated considering the weighed mass. Since, for one mol of the repeating motif there is one mol of JFAED, the number of theoretical moles of the repeating motif was calculated. Finally, with the molar mass of the repeating motif (2958 g/mol), the theoretical mass was calculated and compared with the weight of the recovered polymer to obtain the yield.

- Fourier transform Infrared (FTIR)

Infrared spectra were obtained using a *Bruker Invenio S* with a micro-ATR device. The measurements were performed under dry air atmosphere and the obtained data was treated with the OPUS software.

- Proton nuclear magnetic resonance (^{1}H NMR)

^{1}H NMR analyses were conducted to verify the chemical structure and the stoichiometry of the different monomer units in the polymer. Around 15 mg of polymer were dissolved in 0.7 ml of DMSO-d6. The measurements were carried out with a Bruker AvanceNeo 400 at 400.18 MHz. The data treatment was developed with the TOPSIN software.

2.1.1.2. MMM

2.1.1.2.1. MMMs elaboration

Before elaborating the membranes, it was necessary to perform some calculations to define the mass of the ZIF-8 filler according to the target volume fraction (Table 7). A value of 0.35 g/cm^3 was considered for the density of the ZIF-8 particles [76], and a value of 1.3 g/cm^3 for the linear PUI (former determination at LCPM for closely related PUIs). For the different ZIF-8 loadings, with a constant polymer mass value of 0.7g the following data was obtained.

Table 7. Mass and ZIF-8 volume fraction

ZIF-8 volume fraction	Theoretical Mass ZIF-8 (g)	Experimental Mass ZIF-8 (g)
0.1	0.021	-
0.2	0.047	0.0469
0.3	0.081	0.0802
0.4	0.126	0.1263
0.5	0.188	0.1887
0.6	0.283	0.282
0.7	0.440	0.4397

To ensure safe handling of ZIF-8, the team adhered to the nanoparticle safety protocols established by the French Institute for Occupational Safety and Health (INRS), despite the particle size being in the micrometer range. The required personal protective equipment (PPE) included a laboratory coat (worn over a standard coat), a mob cap, shoe covers, a double pair of gloves, protective goggles, and an FFP3 face mask (specifically, the 3M 4279+ model).

Initially, 0.7 g of PUI were dissolved in 15 mL of chloroform in a 25 mL flask (flask 1). The solution was stirred until complete dissolution of the polymer was achieved. To remove potential dust particles and microgels, the polymer solution was filtered through cotton before further use.

In a separate 25 mL flask, ZIF-8 was redispersed in 5 mL of chloroform (flask 2) using an ultrasonic bath (37 Hz, 80% power) maintained at an ice-water temperature for 15 min. Following this step, 1 mL of the polymer solution (from flask 1) was transferred into the second flask, a step referred to as simple

priming, which facilitates the pre-coating of the filler particles with the polymer to enhance compatibility between the filler and the polymer matrix. The dispersion was further homogenized in the ultrasonic bath under the same conditions for an additional 15 min.

In order to enhance the compatibility between ZIF-8 and the continuous phase, among the different techniques available to improve it (such as increasing viscosity to reduce sedimentation of the dispersed particles, priming, and filler modification [77]), priming was selected. The team performed a design of experiments in which the visual aspects of the membranes were evaluated, including the surface roughness of the fabricated membranes as well as SEM-EDX images, to verify the good dispersion of the particles. Therefore, the simple priming technique was applied for ZIF-8 volume fractions ranging from 10% to 40%. For higher filler loadings, double priming (for 50% vol.) and triple priming (for 60% and 70% vol.) were employed to ensure uniform dispersion. After the priming process, the remaining polymer solution (flask 1) was added to the primed ZIF-8 suspension (flask 2). The final mixture was then subjected to ultrasonic homogenization under the previously defined conditions for 60 min to ensure optimal dispersion of the filler within the polymer matrix.

The obtained suspension was poured into a Teflon mold with a 60 mm diameter. The horizontality of the mold was verified before pouring the solution. Then, the solvent was slowly evaporated in an autoclave for 48 h at room temperature. The final drying was carried out under vacuum and at 60°C for 15 h.

2.1.1.2.1. MMMs characterization

- Electronic scanning microscopy and energy-dispersive X-ray (SEM/EDX)

The cross-section and surface images of the membranes were obtained with the scanning electron microscope (SEM) JEOL JSM-6490LV at 5kV. This SEM was combined with an energy-dispersive X-ray (EDX) imaging of Zn atoms that are present in the ZIF-8. The cross-section images were obtained with samples that were freeze-fractured after being immersed in liquid nitrogen. With the aim of having a better identification of the Zn particles, EDX images were retreated with an image format /transparency coefficient of 15%.

- Thermogravimetric analysis (TGA)

Thermogravimetric analyses were performed with a SERATAM analyzer between 20 to 1000°C, with an increase of temperature of 5°C per minute. The data acquisition Software was Setsoft 2000.

- Differential scanning calorimetry (DSC)

DSC measurements were performed with a TA Instruments DSC Q2000. Two heating and cooling cycles were executed between -80°C and 200°C. The second heating cycle was the one chosen for further analysis. Glass transition temperatures were calculated at the transition mid-point with the TA Instrument data treatment software.

2.1.2. Results

2.1.2.1. Polymer

- Yield

The results for the syntheses are summarized in Table 8.

Table 8. Polymer's yield.

Polymer	Experimental JFAED (g)	Experimental MDI (g)	Experimental 6-FDA (g)	Theoretical polymer mass (g)	Experimental polymer mass (g)	Yield (%)
MV1	5.0292	1.2027	1.06409	7.079	5.69	80.3
MV2	5.3509	1.2782	1.1371	7.5318	5.8447	77.6
MV4	5.0095	1.19517	1.06278	7.0512	6.3325	89.8
MV5	5.0038	1.20509	1.11787	7.04326	6.283	89.2
MV6	5.0153	1.20945	1.09572	7.05942	6.3428	89.8

For the syntheses MV1 and MV2, the copolymer yields were unusually low (around 80%). Moreover, the appearance of MV2 was different from what was expected; it did not have the characteristic yellowish color but a green color. In addition, the surface of the polymer was rough and not smooth (as it should be because of its film-forming properties). Regarding the synthesis of MV3, it was not accomplished because it was decided to restart the synthesis of the polymer with some changes in the protocol due to problems with MV1 and MV2 copolymers.

In particular, the filtration of the polymers MV1 and MV2 was not successful during membrane elaboration; a large amount of microgels were present in the solution, hindering the filtration process. It turned out that the conditions for the syntheses of MV1 and MV2 were wrong, the reaction mixtures having been improperly heated because they were not well immersed in the thermal bath. Furthermore, the likely JFAED2000 partial contamination by water (it was an “old” sample dehydrated in 2021) may also have contributed to the partial cross-linking of the copolymers MV1 and MV2. For the sake of timing convenience, the precipitation of MV1 and MV2 was carried out after 2 days of refrigeration of the reaction mixture, which may have also favored cross-linking reactions involving the terminal isocyanate groups and the urea groups.

Finally, for all these reasons, it was decided to restart the syntheses of the copolymer (syntheses of the copolymers MV4, MV5, and MV6) with a freshly dehydrated JFAED2000, taking care to properly immerse the reaction mixture in the heating bath and to precipitate the copolymers immediately after the syntheses.

With all these changes, the copolymer yields greatly increased and reached values of ca. 90%, as was expected from the former work of Solimando et al., (2017). Furthermore, the MV4, MV5, and MV6 polymer filtrations were carried out with no problem (no formation of major microgels in the solution), allowing the elaboration of the different composite membranes. In Table 7 a summary of all the key parameters of the polymer synthesis.

- Fourier transform Infrared (FTIR)

This technique was used in order to validate the stoichiometry of the synthetized polymer. The obtained spectrum of MV5 is represented in Figure 10. The characteristic bands of the polymer are divided into 3 categories corresponding to the 3 main chemical groups present in the copolymer: urea, imide, and ether. For the urea, 3 main bands are identified: at 3283 cm^{-1} (ν_{NH}), at 1650 cm^{-1} (amide I), and at 1540 cm^{-1} (amide II). Regarding the imide, 5 bands are identified: 1781 cm^{-1} (ν_{CO}), 1724 cm^{-1} (amide I), 1511 cm^{-1} (amide II), 1375 cm^{-1} (ν_{CN}), 722 cm^{-1} (δ_{CO}). The bands amide I and amide II have been named by analogy with the corresponding bands for an amide group, as it is usually done for imide and urea groups. Finally, the ether band of the JFAED 2000 is placed at 1090 cm^{-1}, characteristic of the soft block of the polymer.

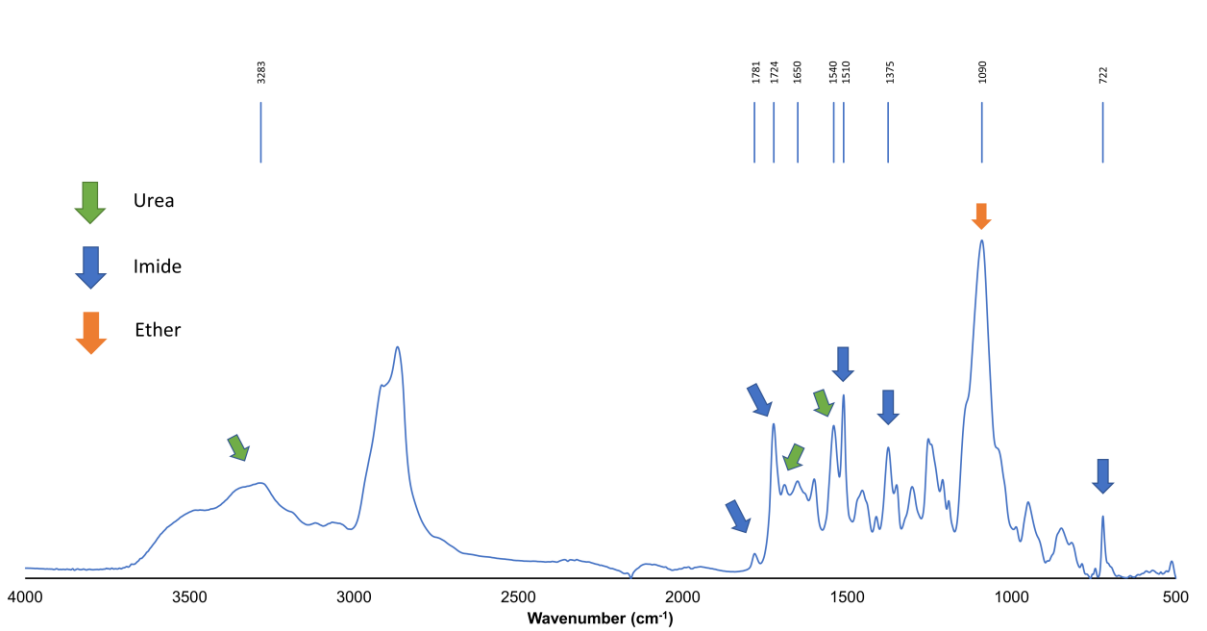

Figure 10. FTIR spectrum of Linear PUI after precipitation

- Proton nuclear magnetic resonance (^{1}H NMR)

The assignment of the different protons was made in good agreement with the formerly published work (Solimando *et al.,* 2017). It confirmed the chemical structure of the different copolymers with protons characteristic for each monomer unit appearing in specific ranges in the ^{1}H NMR spectrum (Figure 11).

Relationships between the number of hydrogens present in the JFAED2000, the MDI, and the 6-FDA monomer units were established to verify the stoichiometry of the copolymer. Two calculation methods were used, they will be detailed for the MV5 synthesis.

The values of x and z (JFAED) were calculated by the team doing an acid-base titration (x+z=5.14). To establish the relationship between the monomers in the repeating unit, for the JFAED 2000, only the protons in the methyl groups (m) were considered, giving a total of 18.42 theoretical protons.

For the 6-FDA, 6 hydrogens are present in the monomer (i,j,k). Regarding the MDI, for the analysis of the spectra, only the protons present on the aromatic rings were considered, giving a total of 16 hydrogens for the two MDI monomers in the repeating unit (a,b,d,e).

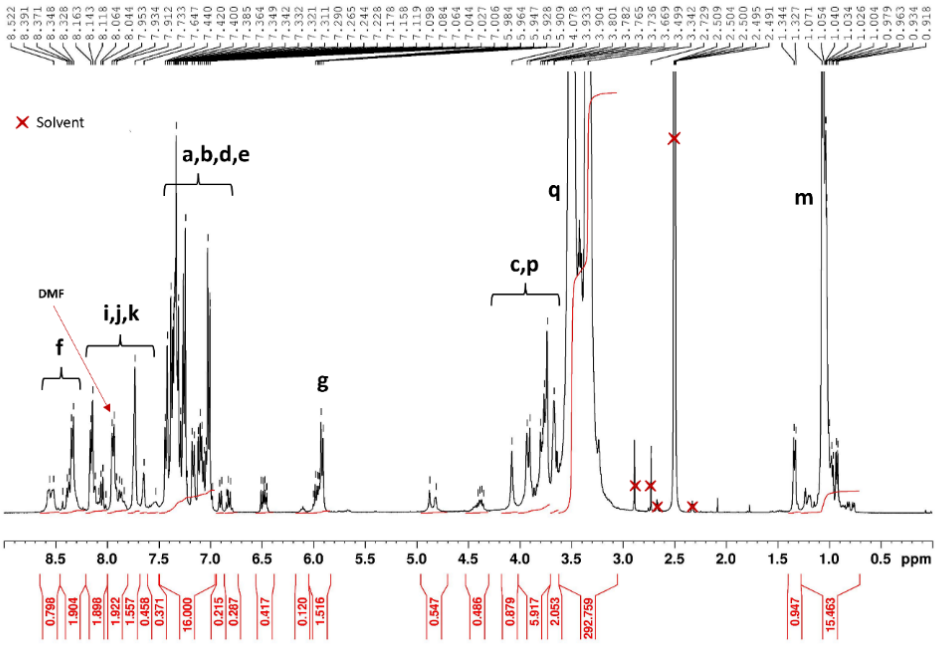

Figure 11. ¹HNMR spectrum of MV5

Among all the analyses made for the different polymer syntheses, residual DMF was detected in the spectra. The peaks that correspond to DMF in the DMSO-d6 are at 2.73 ppm, 2.89 ppm, and 7.95 ppm. The latter is also in a zone where the peaks of the 6-FDA are placed, therefore it was more convenient to analyze the MDI peaks. Nevertheless, it is important to recognize that in the MDI zone of the spectra, there are signals that do not correspond to the monomer, like the labile hydrogens, which may induce a slight error in the estimation of the integration of the MDI aromatic peaks. Moreover, titration is a method that gives a good estimate but not an exact value, in this case of x and z (JFAED), being also a small source of error. Because of all of the factors mentioned before and also of the complexity of the polymer, it is expected an error of around 10%.

Method of calculation

This method is based on a proportionality between the integral of the peaks and the proportion of the number of corresponding protons of these peaks. Theoretically, for 18.42 protons of JFAED, there should be 16 protons that correspond to the two monomer units of the MDI (a,b,d,e,). Then, the MDI/JFAED2000 ratio, should be 2:1. Let us consider X_{JFAED} the number of JFAED2000 units in the copolymer for two MDI monomer units, A1 the area of the JFAED2000 CH_3 protons and A_2 corresponds to the area of the aromatic protons of the two monomer units of the MDI.

$$\frac{A_1}{A_2} = \frac{N°\ protons\ JFAED}{N°\ protons\ MDI} = \frac{[(x+z)*3+3]}{16} X_{JFAED} \tag{18}$$

Taking as an example the polymer MV5. The calculations are as follow:

$$\frac{16.323}{16} = \frac{18.42}{16} X_{JFAED}$$

$$X_{JFAED} = 0.89$$

The error is 11%, showing also by this method that the synthesis was successful.

The results of all the polymer synthesis are summarized in Table 9. In conclusion ^{1}H NMR showed that the synthesized polymers matched the expected stoichiometry and chemical structure apart for copolymer MV2 whose ^{1}H NMR spectrum showed abnormality in the 6-FDA region.

Table 9. Results NMR for the synthesis of the linear PUI

Polymer	JFAED integral	MDI Integral	X_{JFAED}	Experimental Error
MV1	15.978	16	0.87	13%
MV2	16.011	16	0.87	13%
MV4	16.41	16	0.89	11%
MV5	16.323	16	0.89	11%
MV6	15.988	16	0.87	13%

3.1.2.2. Membrane characterization

- Fourier transform Infrared (FTIR)

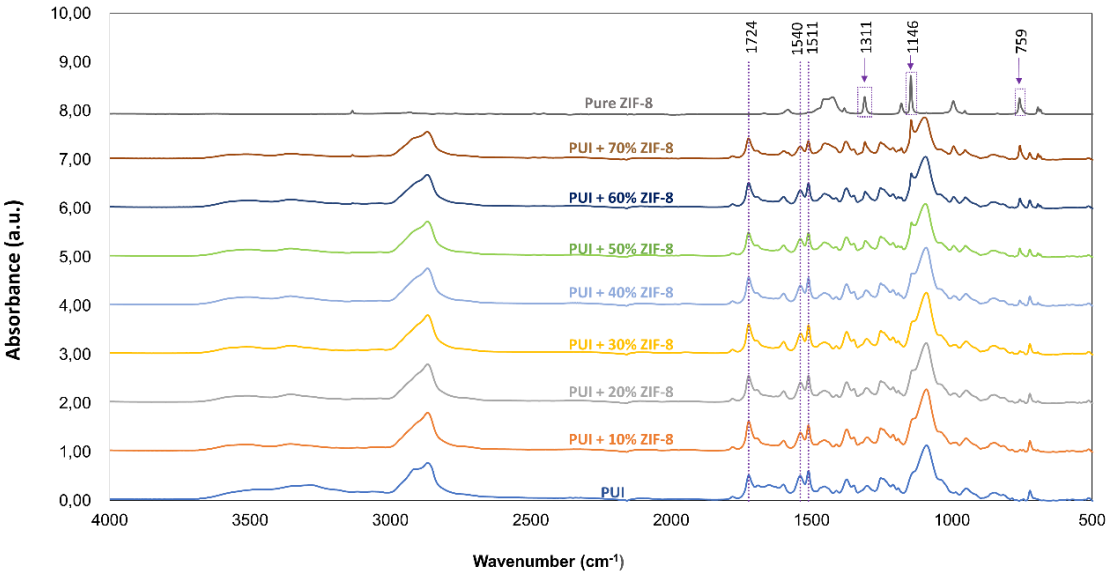

Figure 12. Infrared spectrum of the linear PUI, ZIF-8 and membranes with ZIF-8 charges from 10% to 70%.

The pure polymer, the membranes with different volume fractions of ZIF-8, and the ZIF-8 spectra were stacked and compared. The characteristic bands related to the chemical groups imide and urea of the polymer hard blocks at 1724 cm^{-1}, 1540 cm^{-1}, and 1511 cm^{-1} were present in all the spectrums of the membranes with different volume fractions of ZIF-8 and their wavenumber did not change significantly with the ZIF-8 content (Figure 12). Moreover, the bands with the highest intensity in the ZIF-8 spectrum (1311 cm^{-1}, 1146 cm^{-1}, and 759 cm^{-1}) increased their intensity when the volume fraction of the charge in the membranes increased too. Finally, regarding the band related to the ether groups of the JFAED2000 soft blocks (Figure 13), a shift was observed for the membranes containing at least 50% of

ZIF-8, and this shift increased with the ZIF-8 content. The same trend has also been observed by Kang *et al*. (2020) for MMMs containing ZIF-8 and a polymer matrix made from a SBS-g-POEM copolymer [80]. This shift in the ether band can be due to the interactions between the PUI soft blocks and the fillers, which start to be considerable for high-volume fractions.

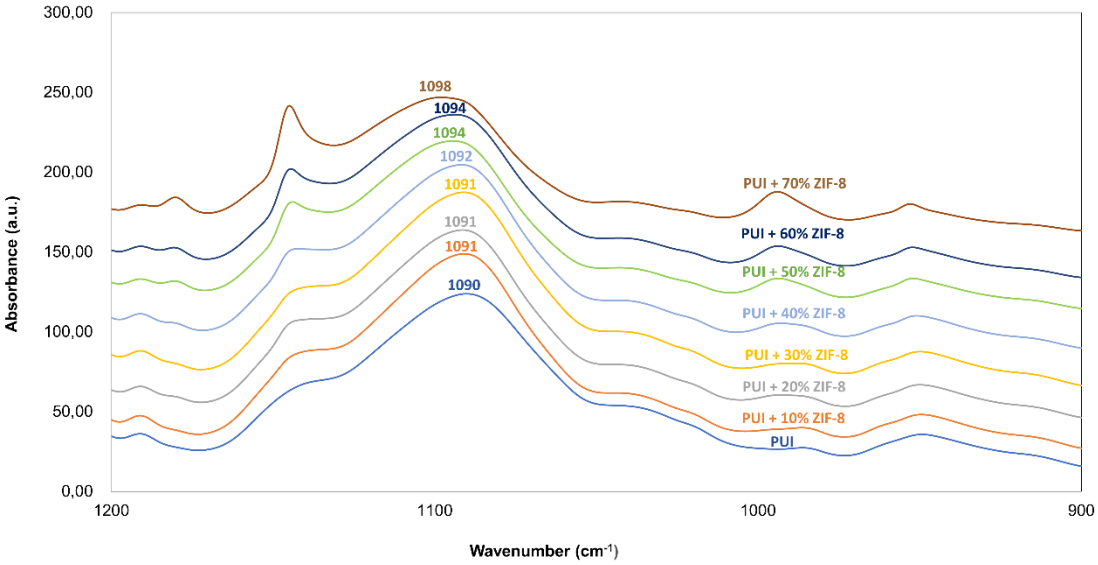

Figure 13. Shift of the ether band for the linear PUI, ZIF-8 and membranes with ZIF-8 from 10% to 70%.

- Electronic scanning microscopy and energy-dispersive X-ray (SEM/EDX)

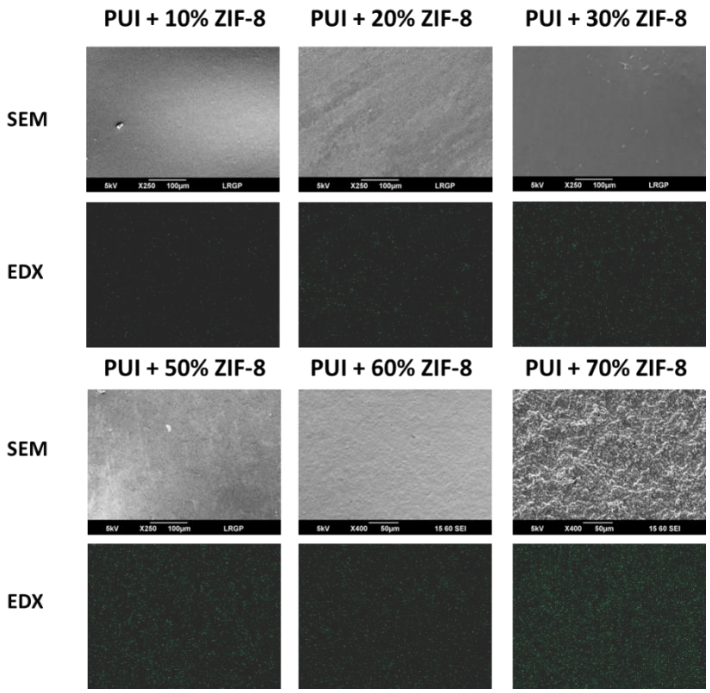

Figure 14. SEM/EDX of membrane surfaces

Based on the SEM results of the membrane surfaces, it can be concluded that increasing the volume fraction of fillers leads to a rougher membrane surface (Figures 14 and 15). Nevertheless, the surfaces were free of major defects.

Moreover, the EDX identified the Zn atoms (which are present in the ZIF-8). It can be observed a higher density of Zinc atoms in the matrix with the increase of the volume fraction of the charge, which is expected. The cross-section images showed the same characteristics as the surface images. For both cases, a homogenous dispersion of the filler is detectable for ZIF-8 contents up to 60%, showing the efficiency of the triple priming for this filler content. Nevertheless, for the membranes with 70% of filler, some agglomerations and voids in the matrix can be seen in the SEM-EDX imaging of the composite membrane.

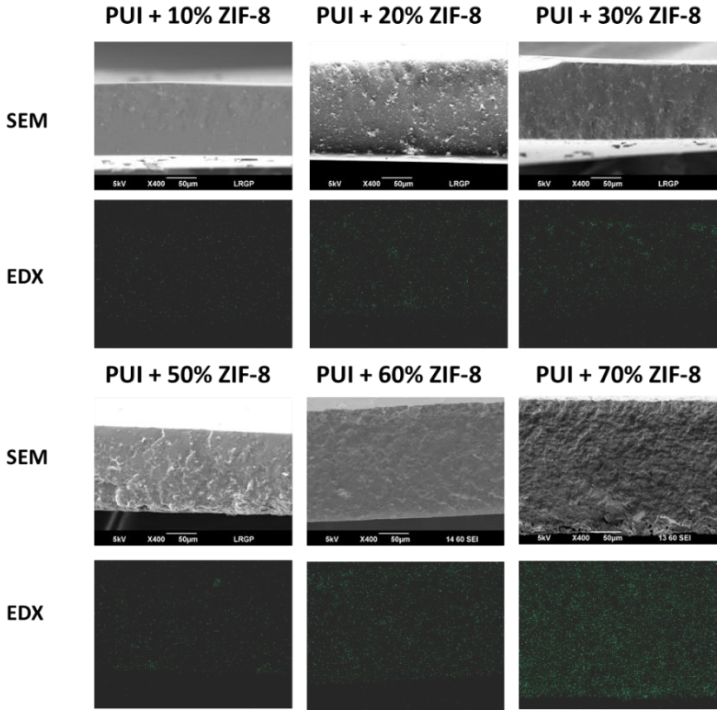

Figure 15. SEM/EDX of membrane cross-sections.

Regarding the classic photos (Figure 16), the transparency of the membranes decreased when the volume fraction of the charges increased. This is because light cannot pass through ZIF-8 particles. Also, some defects on the surfaces of the membranes are detected. They were produced because of the swelling of the materials when they were dried under vacuum; the solvent was coming out of the material and the membranes detached from the Teflon mold generating the defects that can be seen at the border of the membranes.

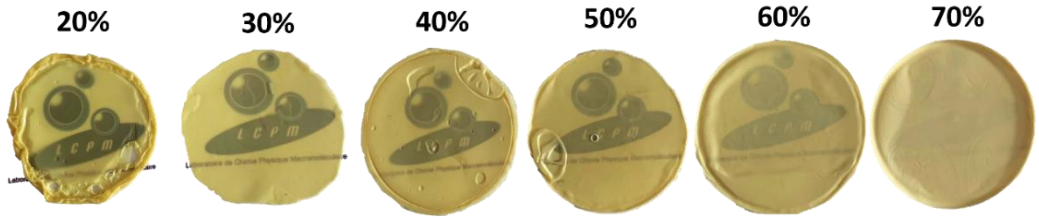

Figure 16. PUI-ZIF-8 Membranes with their ZIF-8 volume fraction.

- Thermogravimetric analysis (TGA)

For all the membranes and the PUI copolymer, a weight loss of less than 5% is presented at temperatures around 200°C. Since the polymer matrix is highly hydrophilic, this is the temperature at which the water molecules absorbed by the PEO are desorbed. Regarding the degradation of the PUI copolymer, it is carried out in two stages; the first one is between 300-400°C and the second one is between 500-550°C. In the first one, the degradation of the soft blocks (JFAED) is carried out. In the second one, the degradation of the hard blocks (MDI/6-FDA) happens.

Also, a right shift of the curves when increasing the volume fraction of ZIF-8 is detected, approaching the curve of the ZIF-8. The decrease in polymer volume fraction is expected as the ZIF-8 volume fraction increases. This means there will be less polymer (organic) and more hybrid material in the MMM. As a result, the weight loss percentage at the same temperature will be lower. With this shift, two zones can be identified. With the materials with a volume fraction of ZIF-8 below 40%, a stronger thermal degradation compared with the behavior of the single polymer matrix is presented. This is a surprising phenomenon that could be explained because of a catalytic effect; Zn atoms are present in the materials, and they could enhance thermo-oxidative degradation of the polymer matrix. For materials with a volume fraction of the fillers over 50%, degradation is diminished compared with the PUI. In this case, the catalytic effect is still present; however, the presence of high filler volume fractions compensates the effect generated by the catalysis, and the membranes try to adopt the degradation behaviour of the ZIF-8; which is clearly more stable than the other analyzed materials presented in Figure 17.

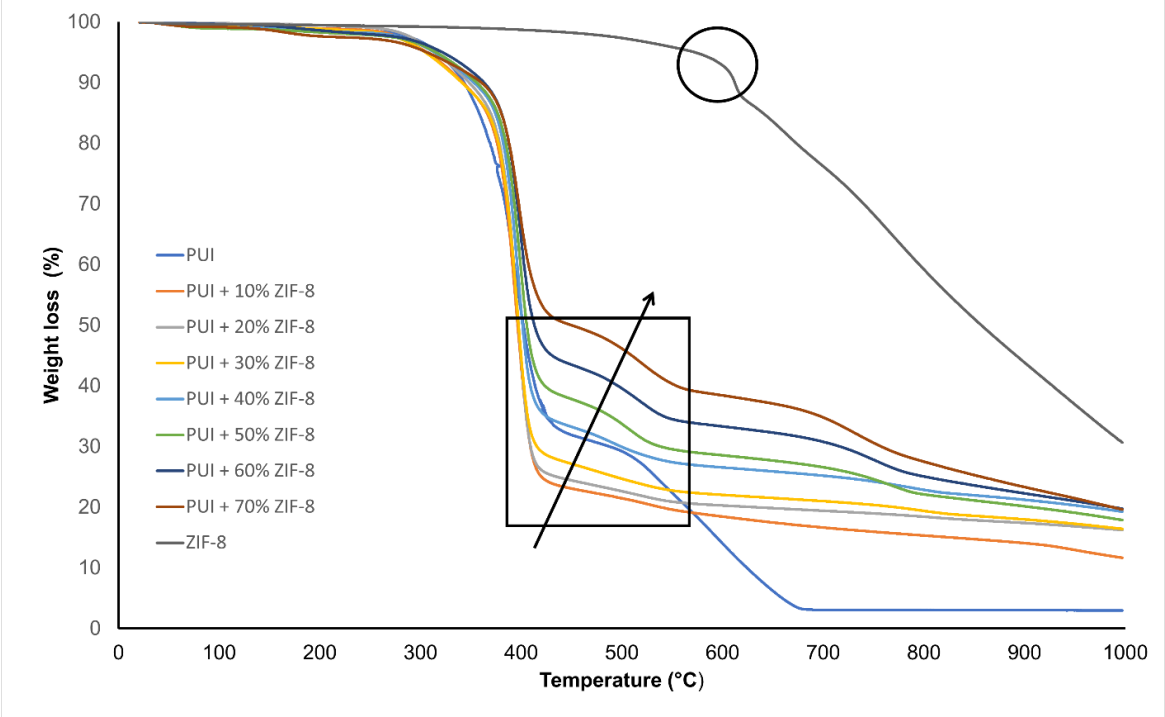

Figure 17. Thermogravimetric analysis of the linear PUI, the membranes with ZIF-8 volume fractions from 10% to 70% and ZIF-8.

- Differential scanning calorimetry (DSC)

With the thermograms that were obtained (Figure 18), only the glassy transition temperature of the soft blocks of the PUI could be identified since the maximum temperature was 200°C (for both, the membranes, and the pure copolymer). This was because the hard block glassy transition temperatures are higher than the decomposition temperature of the soft blocks. Regarding the thermogram of just the copolymer, its glassy transition temperature corresponds to -38°C. Comparing it with the value of the glassy transition temperature of the JFAED2000 (-65°C) [43], the augmentation of the glassy transition temperature for the PUI demonstrated the physical cross-linking generated by the aromatic chemical functions in the copolymer (hard blocks).

Regarding the glassy transition temperature of the soft blocks in the composite membranes, it remained low and did not vary significantly for ZIF-8 contents below 50%. However, from the ZIF-8 volume fraction of 50%, an increase in this parameter was observed. This phenomenon corresponds to the increase of rigidity of the PUI soft blocks with a higher volume fraction of fillers. The results obtained in DSC are well correlated with the shift of the ether band related to the PUI soft blocks for the FTIR spectra, which also started around 40-50% of ZIF-8. Therefore, for high volume fractions of ZIF-8, the interaction between the JFAED2000 soft blocks and the filler particles is stronger, leading to a rigidification of the flexible chains, which is also traduced into an increase of the soft blocks' glassy transition temperature.

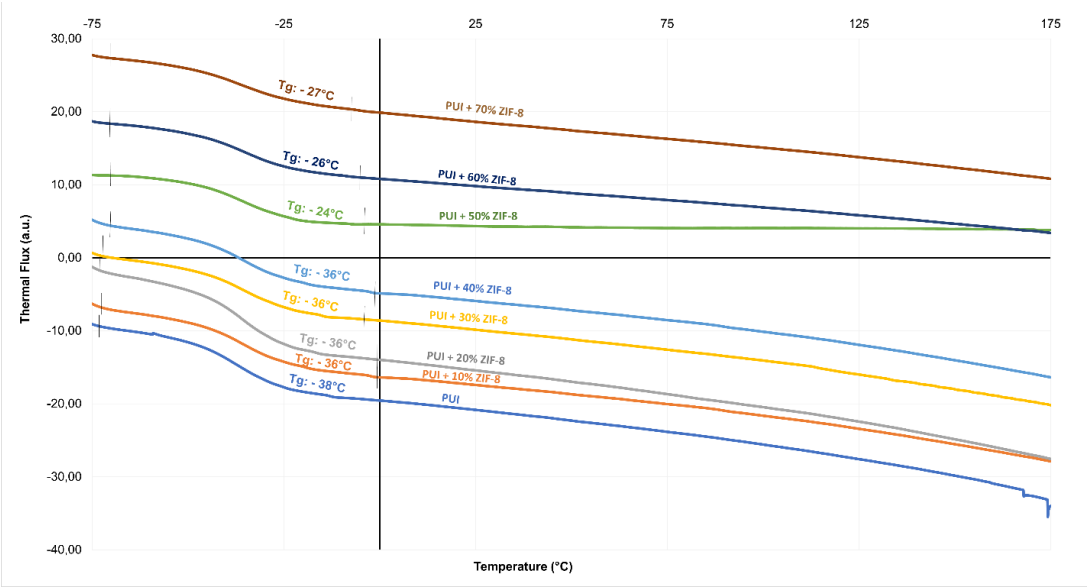

Figure 18. Thermograms (DSC) for PUI and membranes with ZIF-8 from 10% to 70%.

2.2. 2nd Objective: Conduct permeation measurements to obtain CO_2 and N_2 permeability, as well as CO_2/N_2 selectivity.

2.2.1. Methodology

The schematic of the time lag device is shown in Figure 19. Three gas reservoirs (N_2, CO_2, CH_4) are connected to the upstream gas tank via electronically controlled valves (VG1, VG2 and, VG3). Sensor P1 measures the upstream pressure of the cell, while sensor P2 monitors the downstream pressure of the cell.

The permeation measurements started with the measurement of the thickness of the membrane. For this, a precision thickness gauge was used (Elcometer): Around 8 measures in different points of the membrane were carried out on the active area of the membrane (2 cm^2) and the mean value was considered as the average thickness of the MMM. The standard deviation of the membrane thickness was lower than 5 micrometers for membrane thicknesses higher than 100 microns. Then, the membrane was placed in the cell. Afterward, a mode of operation was selected for the automated time-lag, where the number of desired measures, the thickness of the membrane, the time for measurements, and membrane drying were defined. In the first place, the upstream reservoir was filled with the gas to analyze to achieve around 2030-2040 mbar. Since the membranes that were analyzed are very hydrophilic, drying under vacuum for 15 h was conducted to eliminate the possible humidity that the EO groups had absorbed from the synthesis of the material until the permeability tests. For this sequence of the automated operation, the vacuum pump was on, the Evon, MaAPAm, and MaAPAv valves were closed and the VSup and Vinf valves were open to let the upstream and downstream sides of the membrane under dynamic vacuum.

Then, the Evon valve was opened and the Vsup and Vinf valves were closed to measure the leaking rate. An hour was established to obtain stabilized data and then the leaking rate was measured for 150s. Therefore, data on the change of pressure on downstream of the cell over time was registered. With this set of data, the slope of the downstream pressure increase was calculated (this is the leaking rate, useful for further calculations). Then, the permeation measurement started by opening the gas admission valve (Evon). Since the time lag value is unknown, in the first permeation measure a trial and error process with a long measurement time was carried out to identify this parameter and then, the time for the other measures was settled: 10 times the time lag to get enough data in the steady state regime for permeability calculation as explained earlier on. Afterward, all of the steps mentioned before (vacuum drying, measurement of leaking rate, and permeation) were repeated until the total number of measurements was completed. Five measurements were made for each membrane and gas to assess measurement reproducibility, and the average permeability and standard deviation were calculated for each system. For a gas change, the gas tank was emptied under vacuum and then filled with the new gas, and this procedure was repeated twice to be sure to have a pure new gas in the tank. This procedure of gas change was made in an automated way.

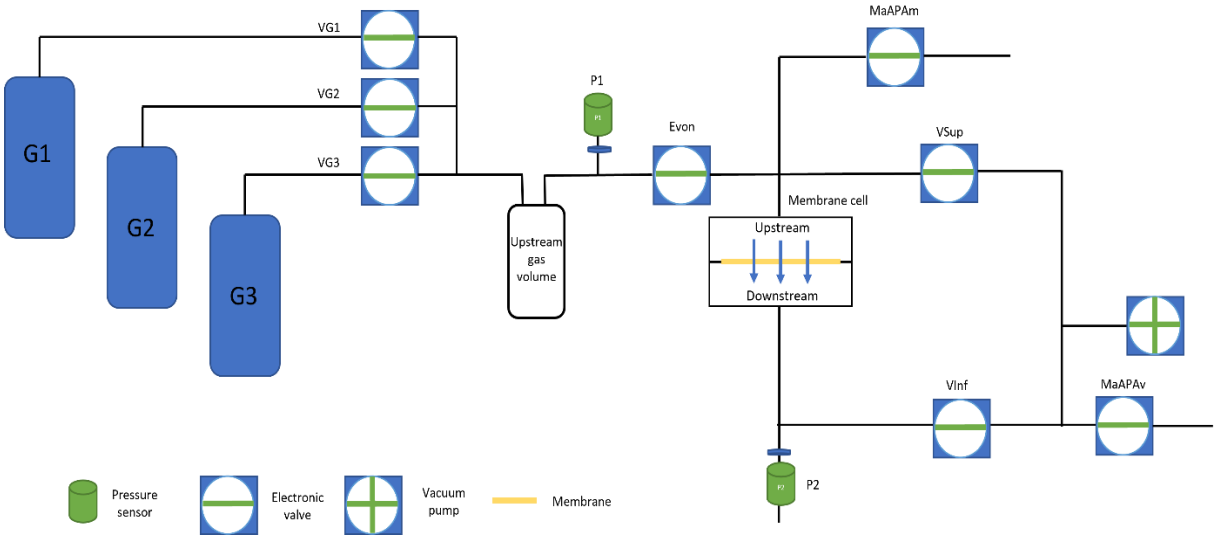

Figure 19. Time-lag set-up. Source: Sivault (2023)

The timing and parameters for each gas used across all membranes are summarized in Table 10. For all materials, a total of five cycles were performed. Prior to each cycle, the membrane was placed in the cell and subjected to an initial vacuum drying step lasting 15 h.

Table 10. Timing for permeation measurements of the PUI JFAED2000 membranes

Gas	Stage	Time
CO_2	Vacuum drying of the material	1 h
	Stabilization	1 h
	Leaking rate	150s
	Permeation measurement	1h
N_2	Vacuum drying of the material	1h
	Stabilization	1h
	Leaking rate	150 s
	Permeation measurement	4 h

This device (Figure 19) was conceived and automated by Jean-Claude SIVAULT, engineer assistant at CNRS, on the basis of the former experience of the team members on time-lag measurements. It is different from the other analog devices that the team had used before because of the fully automatic control system. During the development of this project, the calibration and final upgrades of the device were carried out. In the first place, a polyethylene film was placed inside the cell and data was compiled to adjust and ameliorate the device and automation software. Afterward, calibration with a well-known polymer: PEBAX 1074 was carried out to obtain the downstream volume accessible for the gas (named V2 in the former equations). For performing calibration, the CO_2 permeability of 132.7 Barrer reported in our former work ([42]) was considered and a value of $3.52*10^{-5}$ m^3 was obtained for the downstream volume V2.

2.2.2. Results

Compared to the pristine polymer, the membranes developed in this study demonstrated significantly enhanced carbon dioxide permeability. The most notable increase was observed in the membrane containing 70 vol% ZIF-8, which exhibited a CO_2 permeability nearly eight times higher than that of the pristine polymer (Figure 20). Although a reduction in CO_2/N_2 selectivity was observed with increasing ZIF-8 content, this decline was relatively modest when compared to the substantial gains in permeability. Even at the highest ZIF-8 loading, the selectivity remained above half of that observed in the pristine membrane. This indicates a trade-off primarily driven by the formation of voids at the polymer–filler interface, which facilitates CO_2 transport. However, at high filler loadings, the rigidification of the polymer matrix appears to have partially offset the loss in selectivity by restricting N_2 diffusion more than expected. All of the results of this study for permeability, selectivity, diffusion and solubility for carbon dioxide and nitrogen are presented in the Table 11.

Compared to the pristine polymer, the membranes developed in this study demonstrated significantly enhanced carbon dioxide permeability. The most notable increase was observed in the membrane containing 70 vol% ZIF-8, which exhibited a CO_2 permeability nearly eight times higher than that of the pristine polymer. Although a reduction in CO_2/N_2 selectivity was observed with increasing ZIF-8 content, this decline was relatively modest when compared to the substantial gains in permeability. Even at the highest ZIF-8 loading, the selectivity remained above half of that observed in the pristine membrane. This indicates a trade-off primarily driven by the formation of voids at the polymer–filler interface, which facilitates CO_2 transport. However, at high filler loadings, the rigidification of the polymer matrix appears to have partially offset the loss in selectivity by restricting N_2 diffusion more than expected.

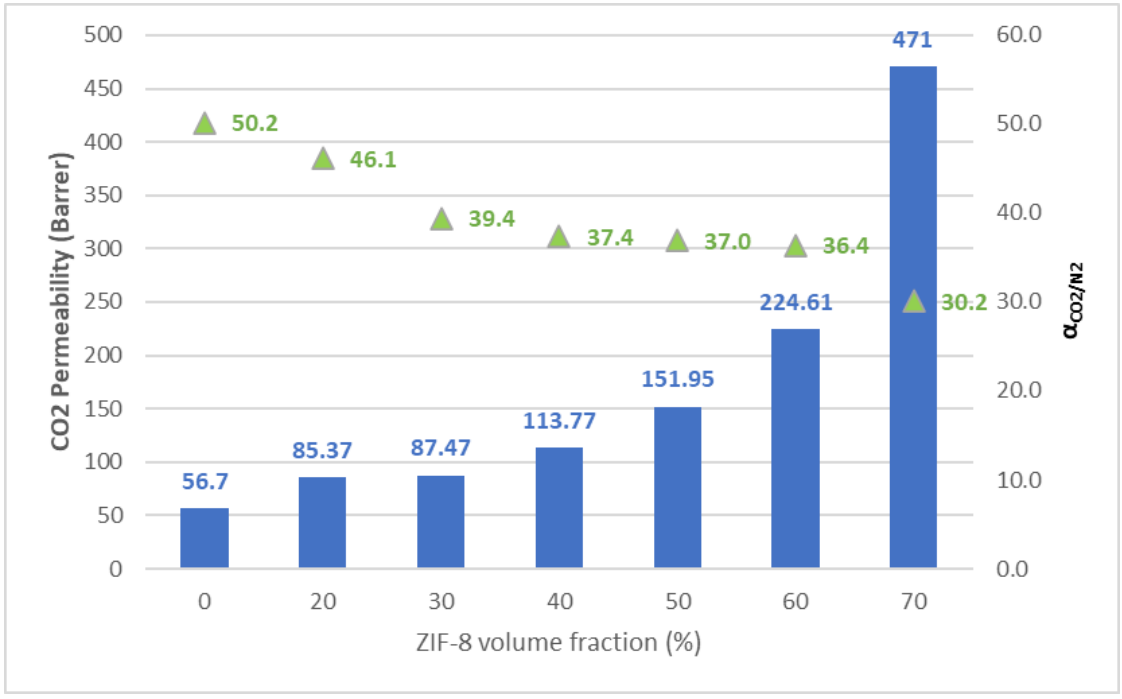

Figure 20. Carbon dioxide permeability (blue bar) and selectivity (green triangles) for the different MMMs with different ZIF-8 volume fractions (0-70%).

Figure 21. Carbon dioxide permeability (blue bar) and selectivity (green triangles) for the different MMMs with different ZIF-8 volume fractions (0-70%).

	P (CO_2) (Barrer)	P (N_2) (Barrer)	D (CO_2) x 10^8 (cm^2/s)	D (N_2) x 10^8 (cm^2/s)	S (CO_2) x 10^3 (cm^3(STP).cm^{-3}.$cmHg^{-1}$)	S (N_2) x 10^3 (cm^3(STP).cm^{-3}.$cmHg^{-1}$)
PUI JFAED 2000	56.7± 2.3	1.13 ± 0.39	26.6± 1.51	18.85± 9.1	21.32	0.6
PUI JFAED 2000 + ZIF-8 (20 % vol)	85.37± 1.9	1.85± 0.04	27.05± 1.9	8.81± 0.09	31.66± 1.5	2.10± 0.04
PUI JFAED 2000 + ZIF-8 (30 % vol)	87.47± 0.2	2.22± 0.05	27.46± 0.24	7.57± 0.27	31.86± 0.23	2.94± 0.04
PUI JFAED 2000 + ZIF-8 (40 % vol)	113.77± 0.2	3.04± 0.25	30.06± 0.19	8.92± 0.3	37.85± 0.21	3.42± 0.3
PUI JFAED 2000 + ZIF-8 (50 % vol)	151.95± 0.4	4.11± 0.03	34.81± 0.43	7.72± 0.09	43.65± 0.65	5.32± 0.09
PUI JFAED 2000 + ZIF-8 (60 % vol)	224.61± 0.3	6.17± 0.27	44.15± 0.21	9.78± 0.23	50.88± 0.24	6.32± 0.4
PUI JFAED 2000 + ZIF-8 (70 % vol)	471± 0.5	15.62± 0.15	105.60± 0.15	21.23± 0.44	44.66± 0.07	7.36± 0.1

Table 11. Influence of the ZIF-8 loading on the CO2 permeability and N2 permeability for the MMMs obtained from the segmented copolymer PUI JFAED2000 at 2 bar and 35 °C

As shown in Figure 21, the CO_2 diffusion coefficient increased exponentially with ZIF-8 content, nearly quadrupling between 20 and 70 vol%. This significant enhancement is likely due to the formation of filler aggregates—clearly visible in SEM images—and the interfacial defects they generate. In parallel, the CO_2 sorption coefficient, calculated from permeability and diffusion data, increased approximately linearly with ZIF-8 content up to 60 vol%, nearly doubling within that range. However, a slight decrease in sorption was noted at 70 vol%, possibly due to increased matrix rigidity limiting gas uptake. Therefore, in membranes containing up to 60 vol% ZIF-8, both sorption and diffusion contributed to the rise in CO_2 permeability. At 70 vol%, however, diffusion—enhanced by aggregate formation—became the dominant transport mechanism.

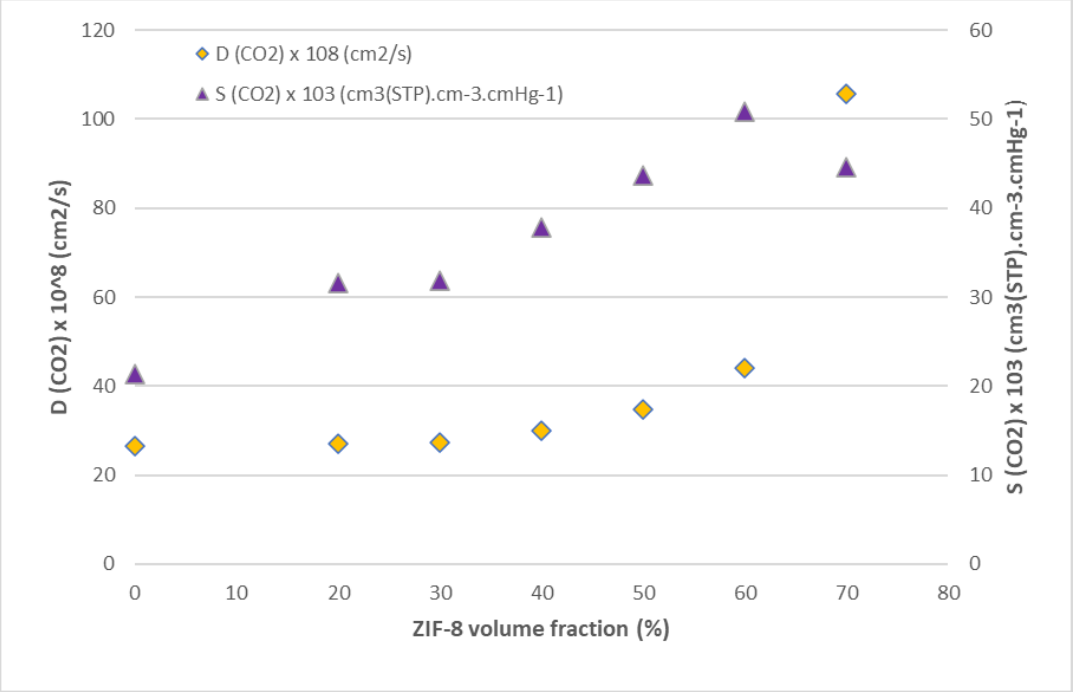

Figure 22. Carbon dioxide sorption (orange) and diffusion (purple) coefficients for carbon dioxide for the different MMMs with ZIF-8 volume fractions from 0-70%.

As shown in Figure 22, the MMMs developed in this study—when compared with other MMMs reported in the literature (summarized in Table 3), featuring different polymer matrices and fillers—demonstrated improved performance in some cases. Notably, the MMM with 70 vol% ZIF-8 approached the Robeson upper bound, indicating a promising balance between permeability and selectivity.

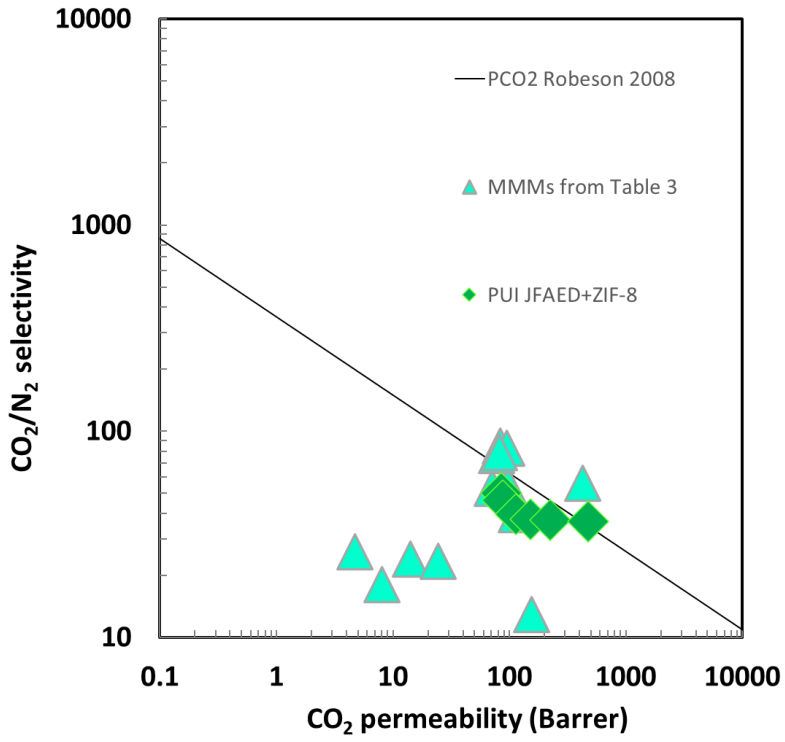

Figure 23. Robeson upper bound and experimental results.

2.3. 3rd Objective: Compare the experimental data with the theoretical values calculated using predictive models.

2.3.1. Methodology

In this study, the models that were studied were presented in the state of art. This analysis was made with the objective of having a deeper understanding of the gas transport properties in MMMs. The maximum packing volume fraction (φ_m) was assumed to be 0.64, which corresponds to the typical value for a random close-packed distribution of uniform spheres [71,75].

To evaluate the accuracy of the permeability models, the average absolute deviation (%AAD) between the experimental and calculated permeability values was calculated for each gas using Equation 19.

$$\%\mathrm{AAD} = \frac{100}{\mathrm{N}} \sum_{\mathrm{i}=1}^{\mathrm{N}} \left| \frac{\mathrm{P_{i,calc}} - \mathrm{P_{i,exp}}}{\mathrm{P_{i,calc}}} \right| \quad (19)$$

For the continuous phase (i.e., polymer matrix) used in this work, the permeability values for carbon dioxide and nitrogen were extracted from Solimando et al., (2017), since the authors developed the exact same polymer matrix studied in this project. Accordingly, the permeability for the CO_2 is 56.7 Barrer and that of N_2 is 1.13 Barrer [42]. For the dispersed phase ZIF-8, the permeability values reported by Diestel et al. (2014) were used: 623 Barrer for CO_2 and 260 Barrer for N_2 [79].

For the resolution of the equations, when they were explicit, the direct formula was used in Excel. For the equations where the permeability was implicit, the Solver function was used to determine the permeability value.

2.3.2. Results

Regarding the comparison with the permeability models (Figures 23 and 24), for filler volume fractions below 30%, all the evaluated models provided comparable estimations of the effective CO_2 permeability. However, beyond 30% filler content, the predictions began to diverge more significantly. Although the Maxwell model is traditionally applied to systems with low filler loadings and does not account for particle shape or interfacial effects in mixed-matrix membranes (MMMs), it demonstrated strong predictive capability for the PUI JFAED 2000 + ZIF-8 system analyzed in this study. Across the full range of ZIF-8 loadings examined, the Maxwell model yielded average absolute deviations (AAD) of 8.5% for CO_2 and 3.5% for N_2 permeabilities. These values—both under 10%—highlight the model's effectiveness in capturing the permeability behavior of pure gases in the MMMs, even at high filler contents up to 60 vol%.

The good modeling by the historical Maxwell model showed that these MMMs behaved as ideal binary systems up to a ZIF-8 loading of 60 % vol and that neither the polymer-filler interactions (revealed by FTIR-ATR) nor the slight increase in the soft block T_g (observed by DSC) significantly impaired this ideal behavior. However, as expected, all models failed to predict the gas permeation behavior of the MMM with the highest ZIF-8 loading (70 % vol).

However, as expected, all models failed to predict the gas permeation behavior of the MMM with the highest ZIF-8 loading (70 % vol). This fact was most likely due to the presence of some aggregates and the related interfacial defects, which strongly increased the diffusion of gas molecules. For the models of Lewis-Nielsen and Pal, it was also related to the inability of these models to make predictions above the theoretical maximum volume fraction of the filler (= 0.64 considered in this work).

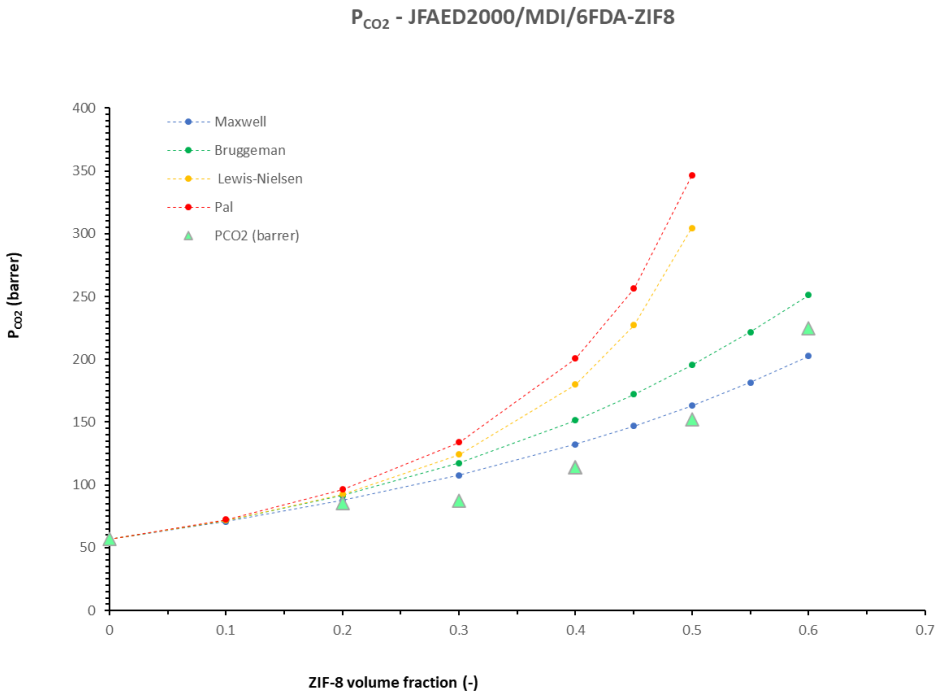

Figure 24. Modeling of carbon dioxide permeability by four semi-predictive ideal models (Maxwell, Bruggeman, Lewis–Nielsen, and Pal) and experimental data for the MMMs obtained from the rubbery segmented copolymer PUI JFAED 2000 and ZIF-8 at 2 bar and 35 °C.

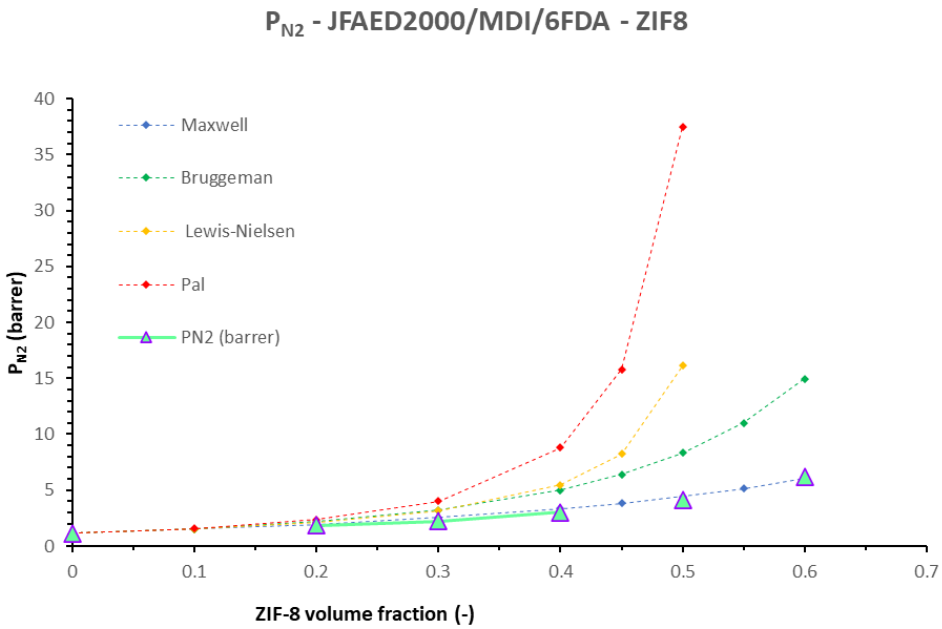

Figure 25. Modeling of nitrogen permeability by four semi-predictive ideal models (Maxwell, Bruggeman, Lewis–Nielsen, and Pal) and experimental data for the MMMs obtained from the rubbery segmented copolymer PUI JFAED 2000 and ZIF-8 at 2 bar and 35°C.

3. Conclusions and perspectives

This study aimed to characterize and evaluate the CO_2 separation performance of mixed-matrix membranes (MMMs) composed of the metal–organic framework ZIF-8 and a newly synthesized multiblock copolymer, PUI JFAED 2000. The successful synthesis of the target copolymer, confirmed by spectroscopic analysis and high mass yields (~90%), enabled the fabrication of dense, homogeneous MMMs with high ZIF-8 loadings—up to 70 vol%—through an optimized priming method. This method proved highly effective in promoting good interfacial compatibility between the polymer matrix and the dispersed filler phase, as evidenced by the absence of major morphological defects and the retention of microphase separation between hard and soft blocks even at high filler contents.

Physicochemical characterization revealed rigidification of the soft blocks of the polymer at high filler content as well as the formation of aggregates. The membrane with 70 vol% ZIF-8 achieved a high CO_2 permeability of 471 Barrer and an ideal selectivity of 30.2 under conditions relevant to post-combustion capture (2 bar, 35 °C), placing it among the top-performing MMMs reported in the literature.

Despite some presence of aggregates and minor interfacial defects, the experimental data up to 60 vol% ZIF-8 aligned well with predictions from the Maxwell model, with average absolute deviations below 10% for both CO_2 and N_2 permeabilities. This demonstrates the model's suitability even for MMMs with relatively high filler loadings.

Future work may focus on more advanced polymer architectures, such as graft copolymers or ternary MMMs to further enhance filler–matrix interactions. Additionally, comparing the experimental results with non-ideal models from effective medium theory could offer deeper insights into interfacial phenomena and defect contributions.

References

[1] United Nations Climate Change, Climate action and support trends, Bonn, 2019.

[2] F. Khosroabadi, A. Aslani, K. Bekhrad, Z. Zolfaghari, Analysis of Carbon Dioxide Capturing Technologies and their technology developments, Clean Eng Technol 5 (2021) 1–17. https://doi.org/10.1016/j.clet.2021.100279.

[3] X. Wang, C. Song, Carbon Capture From Flue Gas and the Atmosphere: A Perspective, Front Energy Res 8 (2020). https://doi.org/10.3389/fenrg.2020.560849.

[4] Y. Keho, What drives energy consumption in developing countries? The experience of selected African countries, Energy Policy 91 (2016) 233–246. https://doi.org/10.1016/j.enpol.2016.01.010.

[5] E. by Bernardo Llamas Moya, J. Pous, Greenhouse Gases, InTech, Zagreb, 2016. https://doi.org/http://dx.doi.org/10.5772/59650.

[6] COP 26 in Glasgow, International Journal of Refrigeration 132 (2021) 5–6. https://doi.org/10.1016/j.ijrefrig.2021.11.029.

[7] R. Cassia, M. Nocioni, N. Correa-Aragunde, L. Lamattina, Climate Change and the Impact of Greenhouse Gasses: CO2 and NO, Friends and Foes of Plant Oxidative Stress, Front Plant Sci 9 (2018). https://doi.org/10.3389/fpls.2018.00273.

[8] J. Skea, R.S. Priyadarshi, A. Reisinger, R. Slade, M. Pathak, A. Al Khourdajie, R. van Diemen, A. Abdulla, K. Akimoto, M. Babiker, Q. Bai, I. Bashmakov, C. Bataille, G. Berndes, G. Blanco, K. Blok, M. Bustamante, E. Byers, L.F. Cabeza, K. Calvin, C. Carraro, L. Clarke, A. Cowie, F. Creutzig, D.K. Dadi, D. Dasgupta, H. De Coninck, F. Denton, S. Dhakal, N.K. Dubash, O. Geden, M. Grubb, C. Guivarch, S. Gupta, A. Hahmann, K. Halsnaes, P. Jaramillo, K. Jiang, F. Jotzo, T.Y. Jung, S. Kahn Ribeiro, S. Khennas, Ş. Kılkış, S. Kreibiehl, V. Krey, E. Kriegler, W. Lamb, F. Lecocq, S. Lwasa, N. Mahmoud, C. Mbow, D. McCollum, J.C. Minx, C. Mitchell, R. Mrabet, Y. Mulugetta, G.-J. an Nabuurs, G. Nemet, P. Newman, L. Niamir, L.J. Nilsson, S.B. Nugroho, C. Okereke, S. Pachauri, A. Patt, R. Pichs-Madruga, J. Portugal Pereira, L. Rajamani, K. Riahi, J. Roy, Y. Saheb, R. Schaeffer, K. Seto, S. Some, L. Steg, F. L. Toth, D. Ürge-Vorsatz, D. Van Vuuren, E. Verdolini, P. Vyas, Y.-M. Wei, M. Williams, H. Winkler, Mitigation of Climate Change 2022 Working Group III contribution to the Sixth Assessment Report of the Intergovernmental Panel on Climate Change, 2021. https://www.ipcc.ch/site/assets/uploads/2018/05/uncertainty-guidance-note.pdf.

[9] G.A. Schmidt, R.A. Ruedy, R.L. Miller, A.A. Lacis, Attribution of the present-day total greenhouse effect, J Geophys Res 115 (2010) 1–6. https://doi.org/10.1029/2010JD014287.

[10] K.S. Nielsen, P.C. Stern, T. Dietz, J.M. Gilligan, D.P. van Vuuren, M.J. Figueroa, C. Folke, W. Gwozdz, D. Ivanova, L.A. Reisch, M.P. Vandenbergh, K.S. Wolske, R. Wood, Improving Climate Change Mitigation Analysis: A Framework for Examining Feasibility, One Earth 3 (2020) 325–336. https://doi.org/10.1016/j.oneear.2020.08.007.

[11] D. Gielen, F. Boshell, D. Saygin, M.D. Bazilian, N. Wagner, R. Gorini, The role of renewable energy in the global energy transformation, Energy Strategy Reviews 24 (2019) 38–50. https://doi.org/10.1016/j.esr.2019.01.006.

[12] M. Hafner, S. Tagliapietra, M.-A. Eyl-Mazzega, C. Mathieu, J. Elkind, The European Union and the Energy Transition- US Clean Energy Transition and Implications for Geopolitics, in: M. Hafner, S. Tagliapietra (Eds.), The Geopolitics of the Global Energy Transition, Springer Nature Switzerland AG, Cham, 2020: pp. 1–47. http://www.springer.com/series/8874.

[13] J. Vansant, Carbon dioxide emission and merchant market in the european union, in: M. Aresta (Ed.), Carbon Dioxide Recovery and Utilization, Kluw er Acad em ie Publish ers, Heusden Zolder, 2003: pp. 3–50.

[14] Y. Wang, L. Zhao, A. Otto, M. Robinius, D. Stolten, A Review of Post-combustion CO2 Capture Technologies from Coal-fired Power Plants, in: Energy Procedia, Elsevier Ltd, 2017: pp. 650–665. https://doi.org/10.1016/j.egypro.2017.03.1209.

[15] E. Martin-Roberts, V. Scott, S. Flude, G. Johnson, R.S. Haszeldine, S. Gilfillan, Carbon capture and storage at the end of a lost decade, One Earth 4 (2021) 1569–1584. https://doi.org/10.1016/j.oneear.2021.10.002.

[16] P. Gabrielli, M. Gazzani, M. Mazzotti, The Role of Carbon Capture and Utilization, Carbon Capture and Storage, and Biomass to Enable a Net-Zero-CO2 Emissions Chemical Industry, Ind Eng Chem Res 59 (2020) 7033–7045. https://doi.org/10.1021/acs.iecr.9b06579.

[17] A. Sood, S. Vyas, Carbon Capture and Sequestration- A Review, in: IOP Conf Ser Earth Environ Sci, Institute of Physics Publishing, 2017. https://doi.org/10.1088/1755-1315/83/1/012024.

[18] T.C. Merkel, H. Lin, X. Wei, R. Baker, Power plant post-combustion carbon dioxide capture: An opportunity for membranes, J Memb Sci 359 (2010) 126–139. https://doi.org/10.1016/j.memsci.2009.10.041.

[19] Y. Han, W.S.W. Ho, Polymeric membranes for CO2 separation and capture, J Memb Sci 628 (2021) 119244 (24). https://doi.org/10.1016/j.memsci.2021.119244.

[20] G. Ji, M. Zhao, Membrane Separation Technology in Carbon Capture, in: Recent Advances in Carbon Capture and Storage, InTech, 2017: pp. 61–90. https://doi.org/10.5772/65723.

[21] M. Wang, A. Lawal, P. Stephenson, J. Sidders, C. Ramshaw, Post-combustion CO2 capture with chemical absorption: A state-of-the-art review, Chemical Engineering Research and Design 89 (2011) 1609–1624. https://doi.org/10.1016/j.cherd.2010.11.005.

[22] M. Ketzer, R. Iglesias, S. Einloft, Advanced Combustion, in: Handbook of Climate Change Mitigation, 2012: pp. 1405–1983.

[23] M.A. Hanif, F. Nadeem, R. Tariq, U. Rashid, Future energy options: an overview, in: Renewable and Alternative Energy Resources, Elsevier, 2022: pp. 113–169. https://doi.org/10.1016/B978-0-12-818150-8.00009-5.

[24] R. Czarnota, E. Knapik, P. Wojnarowski, D. Janiga, J. Stopa, Carbon dioxide separation technologies, Archives of Mining Sciences 64 (2019) 487–498. https://doi.org/10.24425/ams.2019.129364.

[25] R. Kusumastuti, Sriyono, M. Pancoko, S.L. Butar-Butar, G.E. Putra, H. Tjahjono, Study on the Mechanism of CO2 Adsorption Process on zeolite 5A as a Molecular Sieve in RDE System: An Infrared Investigation, in: J Phys Conf Ser, Institute of Physics Publishing, 2019. https://doi.org/10.1088/1742-6596/1198/3/032009.

[26] L. Baxter, C. Hoeger, K. Stitt, S. Burt, A. Baxter, Cryogenic Carbon Capture™ (CCC) Status Report, 2021.

[27] G. Chen, T. Wang, G. Zhang, G. Liu, W. Jin, Membrane materials targeting carbon capture and utilization, Advanced Membranes 2 (2022) 100025. https://doi.org/10.1016/j.advmem.2022.100025.

[28] S. Abdul, R. Khan, Z. Yu, C. Secuianu, S. Sima, Carbon Capture, Phase Equilibria for Carbon Capture and Storage, Carbon and Environment, in: Carbon Capture, 2021: pp. 1–7.

[29] M. Edited by Aresta, Carbon Dioxide Recovery and Utilization, Springer Netherlands, 2003. https://doi.org/10.1007/978-94-017-0245-4.

[30] C. Song, Q. Liu, S. Deng, H. Li, Y. Kitamura, Cryogenic-based CO2 capture technologies: State-of-the-art developments and current challenges, Renewable and Sustainable Energy Reviews 101 (2019) 265–278. https://doi.org/10.1016/j.rser.2018.11.018.

[31] H. Demir, G.O. Aksu, H.C. Gulbalkan, S. Keskin, MOF Membranes for CO2 Capture: Past, Present and Future, Carbon Capture Science & Technology 2 (2022) 100026. https://doi.org/10.1016/j.ccst.2021.100026.

[32] A. Kargari, M.T. Ravanchi, M.O. Adebajo, R.L. Frost, T.L.P. Dantas, A.E. Rodrigues, R.F. Moreira, M. Zoveidavianpoor, A. Samsuri, S.R. Shadizadehand, P.-C. Chen, S. Purtjazyeri, Part 1: Greenhouse Gases - Capturing, Utilization, in: Greenhouse Gases - Capturing, Utilization and Reduction, InTech, 2012: pp. 1–95. https://doi.org/10.5772/2521.

[33] J.G. Wijmans, R.W. Baker, The solution-diffusion model: a review, J Memb Sci 107 (1995) 1–21.

[34] A. Fauzi Ismail, T. Djoko Kusworo, A. Mustafa, H. Hasbullah, Understanding the Solution-Diffusion Mechanism in Gas Separation Membrane for Engineering Students, Proceedings of the 2005 Regional Conference on Engineering Education (2005) 155–159.

[35] L.-M. Sun, J.-Y. Thonnelier, Perméation gazeuse, Procédés Chimie - Bio - Agro | Chimie Verte (2004) J2810 (18).

[36] T.S. Chung, L.Y. Jiang, Y. Li, S. Kulprathipanja, Mixed matrix membranes (MMMs) comprising organic polymers with dispersed inorganic fillers for gas separation, Progress in Polymer Science (Oxford) 32 (2007) 483–507. https://doi.org/10.1016/j.progpolymsci.2007.01.008.

[37] D.Q. Vu, W.J. Koros, S.J. Miller, Mixed matrix membranes using carbon molecular sieves I. Preparation and experimental results, J Memb Sci 211 (2003) 311–334.

[38] M. Vinoba, M. Bhagiyalakshmi, Y. Alqaheem, A.A. Alomair, A. Pérez, M.S. Rana, Recent progress of fillers in mixed matrix membranes for CO2 separation: A review, Sep Purif Technol 188 (2017) 431–450. https://doi.org/10.1016/j.seppur.2017.07.051.

[39] M. Anderson, H. Wang, Y.S. Lin, Inorganic membranes for carbon dioxide and nitrogen separation, Reviews in Chemical Engineering 28 (2012) 101–121. https://doi.org/10.1515/revce-2012-0001.

[40] M. Pera-Titus, Porous inorganic membranes for CO2 capture: Present and prospects, Chem Rev 114 (2014) 1413–1492. https://doi.org/10.1021/cr400237k.

[41] S. Li, Y. Liu, D. Wong, J. Yang, Recent advances in polymer-inorganic mixed matrix membranes for co2 separation, Polymers (Basel) 13 (2021). https://doi.org/10.3390/polym13152539.

[42] X. Solimando, J. Babin, C. Arnal-Herault, M. Wang, D. Barth, D. Roizard, J.R. Doillon-Halmenschlager, M. Ponçot, I. Royaud, P. Alcouffe, L. David, A. Jonquieres, Highly selective multi-block poly(ether-urea-imide)s for CO2/N2 separation: Structure-morphology-properties relationships, Polymer (Guildf) 131 (2017) 56–67. https://doi.org/10.1016/j.polymer.2017.10.007.

[43] V. Muthukumaraswamy Rangaraj, M.A. Wahab, K.S.K. Reddy, G. Kakosimos, O. Abdalla, E.P. Favvas, D. Reinalda, F. Geuzebroek, A. Abdala, G.N. Karanikolos, Metal Organic Framework — Based Mixed Matrix Membranes for Carbon Dioxide Separation: Recent Advances and Future Directions, Front Chem 8 (2020). https://doi.org/10.3389/fchem.2020.00534.

[44] N. Panapitiya, S. Wijenayake, D. Nguyen, C. Karunaweera, Y. Huang, K. Balkus, I. Musselman, J. Ferraris, Compatibilized immiscible polymer blends for gas separations, Materials 9 (2016). https://doi.org/10.3390/ma9080643.

[45] B. Zhu, X. Jiang, S. He, X. Yang, J. Long, Y. Zhang, L. Shao, Rational design of poly(ethylene oxide) based membranes for sustainable CO2capture, J Mater Chem A Mater 8 (2020) 24233–24252. https://doi.org/10.1039/d0ta08806d.

[46] J. Dechnik, J. Gascon, C.J. Doonan, C. Janiak, C.J. Sumby, Mixed-Matrix-Membranen, Angewandte Chemie 129 (2017) 9420–9439. https://doi.org/10.1002/ange.201701109.

[47] B. Xue, X. Li, L. Gao, M. Gao, Y. Wang, L. Jiang, CO 2-selective free-standing membrane by self-assembly of a UV-crosslinkable diblock copolymer, J Mater Chem 22 (2012) 10918–10923. https://doi.org/10.1039/c2jm31037f.

[48] M.R.A. Hamid, H.K. Jeong, Recent advances on mixed-matrix membranes for gas separation: Opportunities and engineering challenges, Korean Journal of Chemical Engineering 35 (2018) 1577–1600. https://doi.org/10.1007/s11814-018-0081-1.

[49] J. Shen, G. Liu, K. Huang, Q. Li, K. Guan, Y. Li, W. Jin, UiO-66-polyether block amide mixed matrix membranes for CO2 separation, J Memb Sci 513 (2016) 155–165. https://doi.org/10.1016/j.memsci.2016.04.045.

[50] A.J. Brown, J.R. Johnson, M.E. Lydon, W.J. Koros, C.W. Jones, S. Nair, Continuous polycrystalline zeolitic imidazolate framework-90 membranes on polymeric hollow fibers, Angewandte Chemie - International Edition 51 (2012) 10615–10618. https://doi.org/10.1002/anie.201206640.

[51] H. Daglar, S. Keskin, High-Throughput Screening of Metal Organic Frameworks as Fillers in Mixed Matrix Membranes for Flue Gas Separation, Adv Theory Simul 2 (2019) 1900109 (11). https://doi.org/10.1002/adts.201900109.

[52] A.G. Kontos, V. Likodimos, C.M. Veziri, E. Kouvelos, N. Moustakas, G.N. Karanikolos, G.E. Romanos, P. Falaras, CO2 captured in zeolitic imidazolate frameworks: Raman spectroscopic analysis of uptake and host-guest interactions, ChemSusChem 7 (2014) 1696–1702. https://doi.org/10.1002/cssc.201301323.

[53] W. Zheng, R. Ding, K. Yang, Y. Dai, X. Yan, G. He, ZIF-8 nanoparticles with tunable size for enhanced CO2 capture of Pebax based MMMs, Sep Purif Technol (2019) 111–119. https://doi.org/10.1016/j.seppur.2018.04.010.

[54] R. Surya Murali, A.F. Ismail, M.A. Rahman, S. Sridhar, Mixed matrix membranes of Pebax-1657 loaded with 4A zeolite for gaseous separations, Sep Purif Technol 129 (2014) 1–8. https://doi.org/10.1016/j.seppur.2014.03.017.

[55] T.H. Lee, A. Ozcan, I. Park, D. Fan, J.K. Jang, P.G.M. Mileo, S.Y. Yoo, J.S. Roh, J.H. Kang, B.K. Lee, Y.H. Cho, R. Semino, H.W. Kim, G. Maurin, H.B. Park, Disclosing the Role of Defect-Engineered Metal–Organic Frameworks in Mixed Matrix Membranes for Efficient CO2 Separation: A Joint Experimental-Computational Exploration, Adv Funct Mater 31 (2021). https://doi.org/10.1002/adfm.202103973.

[56] Y. Zhang, Y. Tong, X. Li, S. Guo, H. Zhang, X. Chen, K. Cai, L. Cheng, W. He, Pebax Mixed-Matrix Membrane with Highly Dispersed ZIF-8@CNTs to Enhance CO2/N2Separation, ACS Omega 6 (2021) 18566–18575. https://doi.org/10.1021/acsomega.1c00493.

[57] L. Dong, M. Chen, J. Li, D. Shi, W. Dong, X. Li, Y. Bai, Metal-organic framework-graphene oxide composites: A facile method to highly improve the CO2 separation performance of mixed matrix membranes, J Memb Sci 520 (2016) 801–811. https://doi.org/10.1016/j.memsci.2016.08.043.

[58] J. Yuan, H. Zhu, J. Sun, Y. Mao, G. Liu, W. Jin, Novel ZIF-300 Mixed-Matrix Membranes for Efficient CO2 Capture, ACS Appl Mater Interfaces 9 (2017) 38575–38583. https://doi.org/10.1021/acsami.7b12507.

[59] J. Shen, M. Zhang, G. Liu, K. Guan, W. Jin, Size effects of graphene oxide on mixed matrix membranes for CO2 separation, AIChE Journal 62 (2016) 2843–2852. https://doi.org/10.1002/aic.15260.

[60] S. Shen, X. Li, Z. Fang, N. Shen, Effect of Gas Adsorption on the Application of the Pulse-Decay Technique, Geofluids 2020 (2020) (11). https://doi.org/10.1155/2020/8872888.

[61] M.J.C. Ordoñez, K.J. Balkus, J.P. Ferraris, I.H. Musselman, Molecular sieving realized with ZIF-8/Matrimid® mixed-matrix membranes, J Memb Sci 361 (2010) 28–37. https://doi.org/10.1016/j.memsci.2010.06.017.

[62] S. Keskin, S.A. Altinkaya, A review on computational modeling tools for MOF-based mixed matrix membranes, Computation 7 (2019). https://doi.org/10.3390/computation7030036.

[63] J. Feng, S.R. Venna, D.P. Hopkinson, Interactions at the interface of polymer matrix-filler particle composites, Polymer (Guildf) 103 (2016) 189–195. https://doi.org/10.1016/j.polymer.2016.09.059.

[64] H. Vinh-Thang, S. Kaliaguine, Predictive models for mixed-matrix membrane performance: A review, Chem Rev 113 (2013) 4980–5028. https://doi.org/10.1021/cr3003888.

[65] M. Zarabadipoor, S. Maghami, A. Mehrabani-Zeinabad, M. Sadeghi, A comprehensive modeling approach for determining the role and nature of interfacial morphology in mixed matrix membranes, Comput Mater Sci 197 (2021) 110590 (18). https://doi.org/10.1016/j.commatsci.2021.110590.

[66] R. Pal, Permeation models for mixed matrix membranes, J Colloid Interface Sci 317 (2008) 191–198. https://doi.org/10.1016/j.jcis.2007.09.032.

[67] L.G. Toy, B.D. Freeman, R.J. Spontak, A. Morisato, I. Pinnau, Notes Gas Permeability and Phase Morphology of Poly(1-(trimethylsilyl)-1-propyne)/ Poly(1-phenyl-1-propyne) Blends, Macromolecules (1997) 4766–4769.

[68] R.H.B. Bouma, A. Checchetti, G. Chidichimo, E. Drioli, Permeation through a heterogeneous membrane: the effect of the dispersed phase, J Memb Sci 128 (1997) 141–149.

[69] Maithem H - Rasheed, The atomic packing factor [A.P.F], (2023). https://www.uobabylon.edu.iq/eprints/publication_1_2901_199.pdf (accessed April 21, 2023).

[70] J.C. Maxwell, A Treatise on Electricity and Magnetism, Cambridge University Press, 2010. https://doi.org/10.1017/CBO9780511709333.

[71] A. Ebneyamini, H. Azimi, F.H. Tezel, J. Thibault, Mixed matrix membranes applications: Development of a resistance-based model, J Memb Sci 543 (2017) 351–360. https://doi.org/10.1016/j.memsci.2017.08.065.

[72] J.H. Petropoulos, A Comparative Study of Approaches Applied to the Permeability of Binary Composite Polymeric Materials, Journal of Polymer Science: Polymer Physics Edition 23 (1985) 1309–1324.

[73] T.B. Lewis, L.E. Nielsen, Dynamic Mechanical Properties of Particulate-Filled Composites, J Appl Polym Sci 14 (1970) 1449–1471.

[74] A. Idris, Z. Man, A.S. Maulud, F. Uddin, Modified Bruggeman models for prediction of CO2 permeance in polycarbonate/silica nanocomposite membranes, Canadian Journal of Chemical Engineering 95 (2017) 2398–2409. https://doi.org/10.1002/cjce.22933.

[75] R. Pal, New models for thermal conductivity of particulate composites, Journal of Reinforced Plastics and Composites 26 (2007) 643–651. https://doi.org/10.1177/0731684407075569.

[76] Sigma Aldrich, Basolite® Z1200-Sigma Aldrich , Https://Www.Sigmaaldrich.Com/FR/Fr/Product/Aldrich/691348 (2023).

[77] H. Wu, J. Thibault, B. Kruczek, The validity of the time-lag method for the characterization of mixed-matrix membranes, J Memb Sci 618 (2021) 118715 (12). https://doi.org/10.1016/j.memsci.2020.118715.

[78] C. Makhloufi, L. Wang, Time-lag tutorial XXIX EMS summerschool on membranes, in: 2012. http://www.uni-duesseldorf.de/.

[79] L. Diestel, X.L. Liu, Y.S. Li, W.S. Yang, J. Caro, Comparative permeation studies on three supported membranes: Pure ZIF-8, pure polymethylphenylsiloxane, and mixed matrix membranes, Microporous and Mesoporous Materials 189 (2014) 210–215. https://doi.org/10.1016/j.micromeso.2013.09.012.

[80] D.A. Kang, K. Kim, J.Y. Lim, J.T. Park, J.H. Kim, Mixed matrix membranes consisting of ZIF-8 in rubbery amphiphilic copolymer: Simultaneous improvement in permeability and selectivity, Chemical Engineering Research and Design 153 (2020) 175–186. https://doi.org/10.1016/j.cherd.2019.10.009.